UNIVERSIDAD DE CHILE
FACULTAD DE CIENCIAS FÍSICAS Y MATEMÁTICAS
DEPARTAMENTO DE FÍSICA

ACTIVE MIXTURES INTERACTING WITH WALLS AND ASYMMETRIC OBSTACLES

TESIS PARA OPTAR AL GRADO DE MAGÍSTER EN CIENCIAS, MENCIÓN FÍSICA

MAURICIO NICOLAS ROJAS VEGA

PROFESOR GUIA:
Dr. Pablo de Castro Melo
PROFESOR CO-GUIA:
Dr. Rodrigo Soto Bertrán

MIEMBROS DE LA COMISIÓN:
Dr. María Luisa Cordero Garayar
Dr. Gustavo Düring Hidalgo
Dr. Cynthia J. Olson Reichhardt

Este trabajo ha sido parcialmente financiado por
FONDECYT y Núcleo Milenio Física de la Materia Activa

SANTIAGO DE CHILE
2022

MEZCLAS ACTIVAS INTERACTUANDO CON PAREDES Y OBSTACULOS ASIMÉTRICOS

RESUMEN

La materia activa se compone de un gran número de partículas autopropulsadas, con ejemplos incluyendo colonias de bacterias, manadas de animales y coloides autoforéticos. En esta tesis, estudiamos una mezcla de partículas autopropulsadas "rápidas" y "lentas" en dos escenarios: (i) en presencia de dos paredes planas paralelas y (ii) en presencia de un arreglo regular de grandes obstáculos asimétricos (con forma de medio disco). Para ello, se realizaron simulaciones 2D con partículas activas Brownianas. El sistema tiene dos tipos de partículas, cada uno caracterizado por su propia velocidad de autopropulsión. Para aislar los efectos de la diversidad en las velocidades, el promedio de las velocidades de autopropulsión se mantiene constante mientras el grado de diversidad es variado. Debido a su movimiento persistente, las partículas se acumulan cerca de los objetos en un fenómeno conocido como mojado. Dado que las partículas rápidas tienen mayor probabilidad de ocupar los espacios disponibles, surge segregación espacial. Cuando la diversidad de velocidades es mayor al 30%, se observa una transición donde la velocidad de autopropulsión de las partículas lentas se vuelve demasiado débil y comienzan a acumularse sobre la "capa" de partículas rápidas en vez de cerca de la pared. Para las paredes planas, encontramos que el proceso de segregación evoluciona en dos etapas: una dinámica rápida, donde la capa de mojado crece a través de la agregación de particulas rápidas y lentas a diferentes tasas, y una dinámica lenta, caracterizada por la relajación de la capa de mojado hacia el estado estacionario. Además, se extendió una teoría cinética previamente usada para separación de fases inducida por motilidad para incluir mojado por mezclas activas. Con una excelente concordancia cuantitativa, nuestras simulaciones y teoría muestran que, al incrementar la diversidad de velocidades, el espesor de la capa de mojado decrece fuertemente y su composición se comporta de manera débilmente no-monótona. Para los obstáculos asimétricos, las partículas viajando desde el lado curvo hacia el lado plano del obstaculo con forma de medio disco pasan menos tiempo atrapadas por el obstáculo que las que viajan en sentido contrario. Como resultado, un movimiento dirigido emerge espontáneamente. Encontramos que surge una corriente de rectificación que se amplifica cuando se aumenta el grado de diversidad entre los tipos. En el límite activo-pasivo, las partículas pasivas siguen participando del movimiento dirigido debido a que son arrastradas por las partículas activas. Debido a la segregación, los perfiles de acumulación en el lado plano y en el lado curvo tienen formas distintas. Cerca de las esquinas del obstáculo, se generan dos pares de vórtices que contribuyen a la rectificación. La vorticidad también aumenta con la diversidad de velocidades. Nuestros resultados entregan información útil sobre el comportamiento de la materia activa en entornos complejos.

ACTIVE MIXTURES INTERACTING WITH WALLS AND ASYMMETRIC OBSTACLES

ABSTRACT

Active matter is composed of a large number of self-propelled particles, with examples encompassing bacterial swarms, animal flocks, and autophoretic colloids. In this thesis, we study a mixture of "fast" and "slow" self-propelled particles in two scenarios: (i) in the presence of two parallel flat walls and (ii) in the presence of a regular array of large asymmetric (half-disk shaped) obstacles. For this purpose, 2D simulations of active Brownian particles were carried out. The system has two types of particles, each one characterized by its own self-propulsion speed. To isolate the effects of speed diversity, the system-average self-propulsion speed is kept unvaried as the degree of speed diversity is varied. Due to their persistent motion, particles accumulate around the objects in a phenomenon known as wetting. Stationary segregation arises since faster particles are more likely to occupy new available spaces. For degrees of speed diversity $\geq 30\%$, we observe a transition where the self-propulsion of the slower particles becomes too weak and thus these particles start to accumulate more easily over a "layer" of faster particles rather than near the wall. For the walls, we find that the segregation process evolves in two stages: a fast dynamics, where the wetting layer grows via aggregation of fast and slow particles at different rates, and a slow dynamics, characterized by the relaxation of the thickness and the composition of the wetting layer towards the stationary state. Also, we extended a kinetic theory previously used for motility-induced phase separation in one-component systems in order to include wetting by active mixtures. With excellent quantitative agreement, our simulations and theory show that, by increasing speed diversity, the wetting layer thickness decreases strongly, whereas its composition is weakly non-monotonic. For asymmetric obstacles, particles traveling from the curved to the flat side of the half-disk obstacle spend less time trapped than in the opposite direction. As a result, directed motion emerges spontaneously. We find that the corresponding rectification current is amplified when the degree of speed diversity is increased. In the active-passive limit, the passive particles still undergo directed motion dragged by the active ones. Due to rectification, segregation profiles are different between the curved and flat sides. Near the obstacle corners, pairs of vortices that further contribute to rectification are observed. Their vorticities also increase with speed diversity. Our results provide useful insights into the behavior of active matter in complex environments.

ACKNOWLEDGMENTS

I would like to thank my supervisors Dr. Pablo de Castro and Prof. Dr. Rodrigo Soto for their guidance and support through the course of my Master's investigation. Their passion for science and knowledge inspired me to grow and to set the foundations for my academic path. I want to thank my Professor for his brilliant lectures and talks. You have become a role model in the way I would like to teach. Thank you for accepting me as your student. To my supervisor Pablo de Castro, thank you for your support in this two-year process, for always pushing me to give my best and for providing me with the criticism I needed to hear in order to become a better scientist. Thank you for encouraging me when I felt tired or frustrated. Your support helped me overcome the difficulties I found in the way, making me stronger for what it is to come.

I wanna thank the friends I made while studying Physics at Universidad de Chile: Robert, Luquitas, Peri, Pauli, Paula, Raza and Byron. Thank you for all the ways you made me walk towards personal and professional growth, making me cherish the time at the university, and for sharing your enthusiasm towards science and knowledge. Also I want to thank the entire community of students in Physics of the University for all the inspiration from the older students and the enthusiasm of the ones that just arrived. I am grateful for all the board games, laughs and enthusiastic discussions we shared. You made that breakout room a safe space for me.

I want to give special thanks to Dr. José González from Universidad Nacional Andrés Bello for believing and trusting me by giving me the opportunity to teach at the University. This experience helped me develop soft skills to give better lectures and confirmed my passion for education and desire to keep communicating science. I want to thank my students for their participation and useful feedback. You motivated me to always give my best. Thank you for trusting me to accompany you in your own path towards knowledge.

I want to dedicate this work to our strong and brave LGBTQIA+ community to remind us that no space can exclude us. If you love science and want to walk this path, you are not alone, and although it won't be easy, every day we can work to make it a safer place. I want to thank all my LGBTQIA+ peers, especially Martin, for their support and their collaboration in the process of forging a path for the next generations.

And most Importantly, I want to thank my partner Leonardo for his love and support. I am grateful for the way you helped me get back up when I felt demotivated. Thank you for believing and loving me with such care and patience. You have all my support and I know that together we are unstoppable.

Contents

Chapter 1

Introduction

1.1 Active Matter

The study of Active Matter focuses on systems of self-propelled particles and their emergent phenomena [1]. Many of its new behaviors are relevant to applications ranging from biology to industry [2]. Examples of Active Matter are abundant, including herds and flocks of animals [3–5], cell tissues [6], bacterial colonies [7] and autophoretic colloids [8]. These systems show complex organized behavior and have one feature in common: each self-propelled entity is an independent agent that processes information from its surroundings and consumes energy locally to generate movement. As a result, these systems are intrinsically out-of-equilibrium as each particle has an irreversible dynamics.

1.2 Microswimmers

In this thesis, we are interested in modelling Active Matter systems on the microscopic scale, particularly microswimmers, such as bacteria, plankton, and algae. Nevertheless, the results presented here are expected to be also valid for analogous systems on other scales. Microswimmers are not restricted to living organisms. In the artificial world, a famous example is that of Janus particles [9]. The surface of each of these microparticles is designed to have two distinct physical properties, allowing them to self-propel by generating local gradients of a solute in their

surrounding fluid. Another example are light sailboats [10], which are microscopic swimmers with a wedge shape covered with a reflective surface, so that the momentum change during reflection provides self-propulsion. Microswimmers are one of the main focuses of Active Matter since they are are relatively easy to control. Also, artificial microswimmers offer exciting opportunities for biomedical applications [11] such as drug delivery [12, 13]. As further discussed below, microswimmers typically exhibit persistent motion (more clearly defined in Section 1.4 below) and active diffusion, the latter commonly being orders of magnitude larger than thermal diffusion. They may also be subject to self-propulsion alignment forces.

1.3 Modelling

There are two main frameworks to model active particles (see Fig. 1.1). The first is called Run-and-Tumble particle (RTP), where the swimmer moves in a straight line until it randomly resets its motion direction (i.e., "tumbles"). The tumbles occur stochastically at some rate α and correspond to abrupt changes of direction. Examples of microswimmers that are typically modelled as RTPs include *E. Coli* and *Salmonella*. The second model is called Active Brownian particle (ABP). Here the particle changes its motion direction via angular diffusion, characterized by a diffusion constant η. In this case, the change of direction is smooth, but also stochastic. ABPs are commonly employed to model artificial microswimmers as well as several "smooth-swimming" bacteria and other microorganisms. Using the common assumption that RTPs spend zero time tumbling, i.e., that tumbles are instantaneous, it has been shown in Ref. [14] that the collective behaviors of RTPs and ABPs are equivalent and can be mapped onto one another through $\alpha \leftrightarrow (d-1)\eta$, where d is the spatial dimension. In our work, we will use ABPs, since their implementation is simpler.

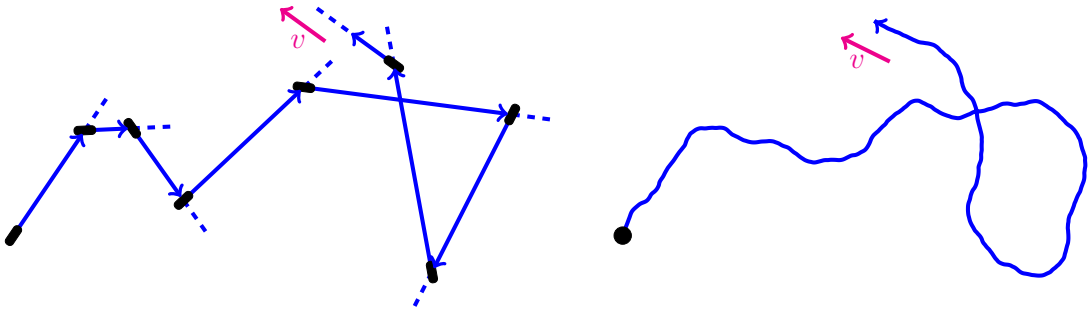

Figure 1.1: Simulated paths of an RTP (left) and an ABP (right). From Ref. [14].

1.4 Collective phenomena

Active particles may interact via alignment forces and/or excluded volume. As a result, interesting fundamental collective behaviors arise. For sufficiently large persistence times or densities, particles do not have time to find an escape route and thus become trapped between other particles. As a result of this trapping mechanism, clusters of active particles surrounded by dilute regions are formed. This phenomenon is called motility-induced phase separation (MIPS) [14]. A phase separation that consists in the formation of clusters of active particles. The key variables that control the presence of MIPS are the persistence of the swimmers, which depends on the reorientation rate and the self-propulsion velocity, and the packing fraction ϕ of the system. Studying a system of ABPs, Ref. [15] showed that ϕ is required to be above $\phi \approx 0.3$ to allow for MIPS. Active matter can also spontaneously accumulate around obstacles even in the absence of attractive forces [16]. This phenomenon arises because active particles normally have a direction of motion that evolves stochastically but slowly, i.e., their direction of motion is *persistent*. Importantly, persistent microswimmers also accumulate in the presence of walls at densities lower than the required to develop MIPS [16]. This is known as active wetting [17–19] and is one of the main subjects of study in this work. Active wetting is interesting since it helps control surface adhesion and capillary properties of bacterial biofilms [20–22], whose formation makes bacterial colonies more resilient

against antibiotics [23]. Although alignment forces are responsible for the emergence of flocking [24], they are not required to generate wetting and are thus neglected here for simplicity. Simulating identical active particles interacting with flat walls, three wetting phases have been identified [25]: complete wetting, incomplete wetting, and complete evaporation (or "unwetting"). On the more theoretical side, a system of ABPs (also one-component) has been studied in Ref. [17] using an effective equilibrium (density functional theory) approach.

In the case of interactions with asymmetric obstacles, i.e., when the interaction is different if the particle moves towards one side or the other, simulations and experiments show that active particles undergo directed motion [26], in addition to accumulation. The spontaneous emergence of net particle transport due to environmental asymmetries, i.e., "rectification" currents, has constituted a central topic in both conceptual and technological contexts for decades [27]. More recently, research on the rectification of self-propelled particles has gained momentum [28–32]. In Ref. [33], an initially homogeneous collection of active Brownian particles in 2D was simulated in a regular array of half-disk rigid obstacles oriented in the same fixed direction. The stationary average speed of the particles was found to be nonzero: instead, an effective rectification current emerges since particles traveling from the curved side to the flat side of the obstacle spend less time trapped than those in the opposite direction. Similar behavior was observed for an irregular array of randomly-located obstacles oriented in the same fixed direction [34]. The sizes of the obstacle and accumulation layers directly affect the intensity of such rectification currents. Rectification by half-disk obstacles shows that no cavity is needed to trap particles [35], meaning that the existence of convex surfaces with distinct curvatures is sufficient to generate currents (see Fig. 1.2).

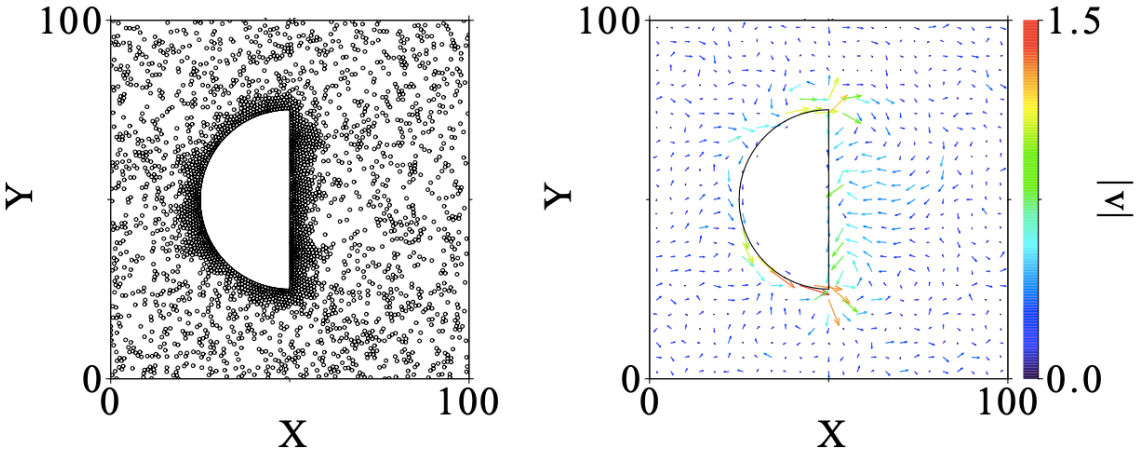

Figure 1.2: A system of identical active Brownian particles accumulating on a convex asymmetric obstacle. Left: Snapshot. Right: Velocity field. From Ref. [33].

1.5 Diversity

Studying active matter interactions with walls and asymmetric obstacles, one typically considers identical active particles, i.e., particles with the same self-propulsion speed, rotational diffusion coefficient, and size. To the best of our knowledge, wetting by active mixtures has not been previously considered in the literature. Similarly, a generalization to active mixtures of the rectification problem shown in Fig. 1.2 has been considered only preliminarily in Ref. [36].

However, diversity is ubiquitous in Nature. For example, in natural colonies of bacteria and other microorganisms, a broad dispersion of motility parameters exists due to different ages, reproduction stages, shapes, sizes, and running modes [35, 37–39]. For either passive or active fluids, it is known that the "diversity" of some particle attribute generates several new phase behavior phenomena, including changing the nature and loci of phase diagram boundaries, and introducing particle-type spatial segregation [18, 24, 40–56]. Therefore, considering diversity in Active Matter systems does not only make our models more accurate but also allows for new associated phenomena.

1.6 Motivation

It remains unclear what are the effects of particle diversity on flat-wall wetting as well as on active rectification by convex asymmetric obstacles. This is important because, in complex biological environments, active matter commonly interacts with obstacles like those, as for example bacteria swimming around the internal structures of the host body where they live [57]. In this work, we give a particular focus to how diversity affects the collective behavior of active matter interacting with surfaces.

1.7 This work & Goals

We will use simulations to investigate a mixture of "fast" and "slow" active Brownian particles, that is, a binary mixture where each particle type is characterized by its own self-propulsion speed, first in the presence of flat walls and then of a regular array of half-disk obstacles. To isolate the effects of such "speed diversity", the system-average self-propulsion speed is kept unvaried as the degree of speed diversity is varied. No external fields, hydrodynamic effects, or imposed alignment rules are present.

Our main objective is to understand how "self-propulsion speed diversity" (hereafter just *speed diversity*) couples with surface interactions in both of our systems. For the flat walls, we want to understand how the thickness and the composition of the wetting layer are affected. For our second model, we will look into how speed diversity affects rectification currents as well as accumulation profiles. In particular, we discuss how these effects are connected with the emergence of segregation in a spectrum of active-active mixtures.

Chapter 2

Model

In experiments with microorganisms, swimming is commonly restricted to 2D due to hydrodynamic attraction in the surrounding fluid towards surfaces [58]. Also, a number of experiments regarding the collective behavior of bacteria are performed in quasi-2D setups [59]. Therefore, since models in two dimensions allow for spatial segregation and are easier to visualize and build intuition on than 3D ones, in this thesis we will work only in 2D. We expect our main qualitative results to be valid in 3D as well.

In this chapter, we describe the key components of our simulations. We will address how we implemented active mixtures, the necessary components to implement the ABP model, and how these active particles interact with each other as well as with the flat walls and the half-disk obstacle.

2.1 Active mixtures

We consider a binary mixture in 2D composed of N active Brownian disks labeled by i, where $N/2$ of them are "fast" particles, with self-propulsion speed $v_i = v_\mathrm{f} \equiv v_0(1+\delta)$, and the other $N/2$ are "slow" particles, with $v_i = v_\mathrm{s} \equiv v_0(1-\delta)$. From now on we will use the subscripts f and s for fast and slow particles respectively . The parameter $\delta \in [0,1]$ thus corresponds to the degree of speed diversity. For $\delta = 0$, all particles have identical self-propulsion speed and the system is called "monodisperse". In the opposite limit, when $\delta = 1$, the mixture is active-passive.

For simplicity, global compositions other than 50-50% are not considered, but generalization is straightforward. On varying δ, the system-average self-propulsion speed is kept at v_0, which is constant and independent of δ. By doing so, the effects of speed diversity can be isolated. To avoid undesired artificial crystallization [60], each particle is randomly assigned one of two diameters, $d_{\text{small}} = d_0$ and $d_{\text{large}} = 1.4d_0$, uncorrelated with particle types. Therefore, there are *four* particle types, but we focus on the effects of speed diversity. The system is said to be just binary or "bidisperse".

The dynamics of each particle's position $\boldsymbol{r}_i$ is governed by the ABPs equations [61]

$$\partial_t \boldsymbol{r}_i = v_i\, \hat{\boldsymbol{\nu}}_i + \mu \boldsymbol{F}_i + \boldsymbol{\xi}_i, \quad \partial_t \theta_i = \eta_i(t), \tag{2.1}$$

where $\hat{\boldsymbol{\nu}}_i = (\cos\theta_i, \sin\theta_i)$ determines the self-propulsion force direction and μ is the mobility. Also, $\boldsymbol{F}_i = \sum_{j\neq i} \boldsymbol{F}_{ij} + \boldsymbol{F}_i^{\text{surface}}$ is the net force on particle i due to interactions with other particles and with flat walls (Chapter 3) or with half-disk shaped obstacles (Chapter 4). The noise terms $\boldsymbol{\xi}_i(t)$ and $\eta_i(t)$ are Gaussian and white, with zero mean and correlations $\langle \xi_{i\alpha}(t)\xi_{j\beta}(t')\rangle = 2\xi\delta_{ij}\delta_{\alpha\beta}\delta(t-t')$ (the Greek letters denote Cartesian coordinates) and $\langle \eta_i(t)\eta_j(t')\rangle = 2\eta\delta_{ij}\delta(t-t')$, where ξ and η are the translational[1] and rotational diffusion coefficients respectively.

The interparticle interactions are taken as a soft repulsive WCA-like potential [62] defined in terms of the interparticle distance r_{ij} as[2]

$$U = \begin{cases} 2^{\frac{3}{2}}\left(\dfrac{\sigma_{ij}}{r_{ij}}\right)^3 - 3\left(\dfrac{\sigma_{ij}}{r_{ij}}\right)^6 + \left(\dfrac{\sigma_{ij}}{r_{ij}}\right)^{12} - \dfrac{3}{4}, & r_{ij} \leq 2^{\frac{1}{6}}\sigma_{ij}, \\ 0, & r_{ij} > 2^{\frac{1}{6}}\sigma_{ij} \end{cases} \tag{2.2}$$

with $\sigma_{ij} \equiv \frac{1}{2}(d_i + d_j)$, where d_i is the particle diameter of particle i.

The parameter distinguishing the particle types is the self-propulsion speed. We choose units and fixed parameters such that $v_0 = 1$ and the diameter scale is $d_0 = 1$.

[1] Besides rotational diffusion, the flat wall problem also includes translational diffusion, which in turn does not affect the qualitative collective behavior. It is included in the model only to make it more suitable for (future) theoretical developments and comparisons.

[2] For similar reasons, the modified WCA potential used here has a smooth second derivative.

For the diffusion coefficients and simulation time step, we use $\xi = 5 \times 10^{-4}$, $\eta = 5 \times 10^{-3}$ and $\Delta t = 5 \times 10^{-4}$. Initially, particles are distributed homogeneously at random positions with random velocity directions, independent of their types. To prevent errors associated with initial overlapping, the inter-particle force is bounded for the first 2 units of simulation time.

2.2 Active mixtures interacting with walls

For our first model we consider mixtures in the presence of two flat walls. For the particle-wall interaction between particle i and any of the sides, d_j is replaced by zero. The simulation is performed in a rectangular box of sides $L_x = 400$ and $L_y = 100$. The walls are located parallel to the y-axis at $x = 195$ and $x = 205$, leaving a space of 10 units of length between them. We consider periodic boundary conditions. The simulation space corresponds to an infinite stripe with soft walls on the sides. The average persistence length of the particles is $\ell \equiv v_0/\eta = 200$, which is comparable to the system size but sufficiently small so that particles are not able move ballistically from one wall to the other, allowing us to treat each wall independently and thus averaging the data from both walls. The occupied area fraction ϕ is defined as the total area occupied by particles divided by the area of the simulation box minus the area between the walls, i.e.,

$$\phi = \frac{N}{2} \times \frac{\frac{\pi}{4}\left(d_{\text{small}}^2 + d_{\text{large}}^2\right)}{L_x L_y - 10 L_y}. \tag{2.3}$$

2.3 Active mixtures interacting with asymmetric obstacle

For our second model, we study the behavior of a mixture in the presence of a half-disk obstacle of radius $D/2$, located at the center of the simulation box with the flat side parallel to the y-axis (as shown in Fig. 1.2). We consider the same type of mixture (without translational diffusion) and time step $\Delta t = 10^{-3}$. For the interaction

with the walls, we use the same potential so that, for the flat side, d_j is replaced by zero and, for the curved wall $d_j = D/2$. Simulations were carried out inside a square box with side $L = 200$ (such that $D = L/2$) and with periodic boundary conditions, simulating therefore an infinite regular array of identical obstacles. Here one has

$$\phi = \frac{N}{2} \times \frac{\frac{\pi}{4}\left(d_{\text{small}}^2 + d_{\text{large}}^2\right)}{L^2 - \frac{\pi}{2}\left(\frac{D}{2}\right)^2}. \tag{2.4}$$

Chapter 3

Active mixtures interacting with walls

The simple model described in Chapter 2 provides a powerful tool to study wetting and segregation in mixtures of active persistent particles. Because of its out-of equilibrium nature, Active Matter shows non-equilibrium steady states (NESS). We divided our analysis for this system into two parts. The first is dedicated to understanding how the system approaches the NESS (transient), and how this is affected by δ; in particular, we will comment on the composition of the wetting layer, its thickness, and the evolution of the orientations of the particles. In the second we study the NESS properties, where we discuss the "equilibrium" composition of the system, its associated concentration profiles, and measure a global segregation parameter, among other analyses. We complement our simulation results with a theoretical approach obtained by extending a kinetic theory previously used for motility-induced phase separation [15] in one-component systems in order to include wetting by active mixtures.

3.1 Transient

Particles start to accumulate quickly on the walls, as shown for $\delta = 0$ and $\phi = 0.18$ in Fig. 3.1 and in our supplementary Movie 3.1. Similarly, Fig. 3.2 and Movie 3.2 show the accumulation for $\delta = 0.5$. The resulting wetting layers are not static: at the interface, particles are constantly being absorbed and emitted; in the inte-

rior, particles are constantly exchanging positions, which can be attributed to their persistent movement.

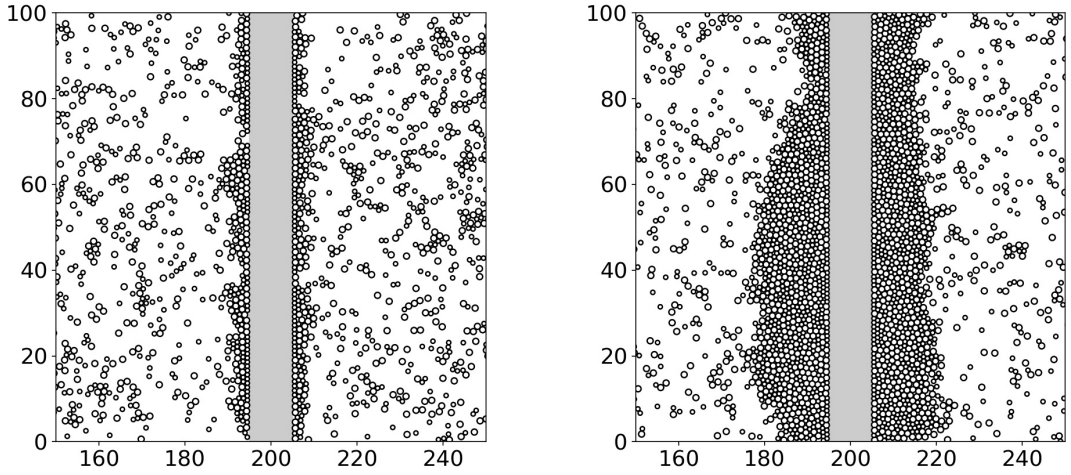

(a) $t = 50$ (b) $t = 250$

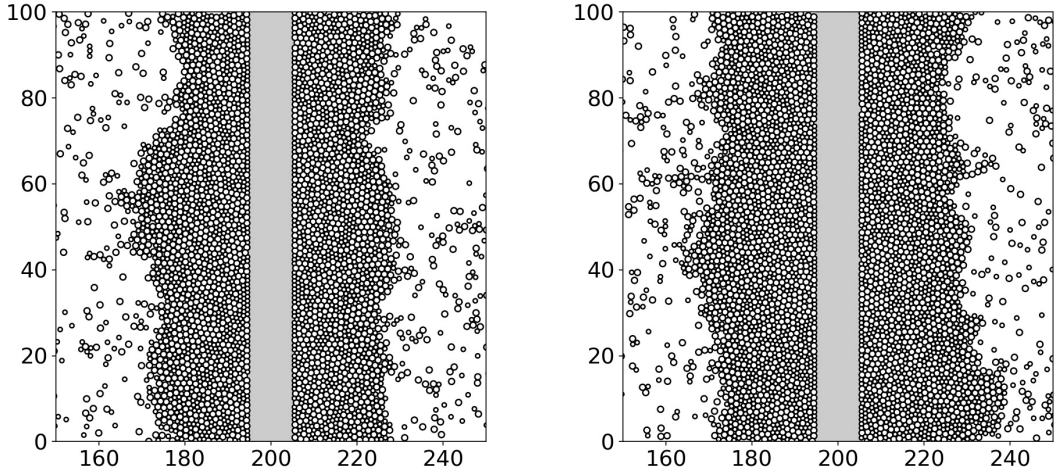

(c) $t = 500$ (d) $t = 1000$

Figure 3.1: Time evolution snapshots for $\delta = 0$ and $\phi = 0.18$. Only a portion of the simulated rectangular box is shown. Values for the other parameters are given in Chapter 2.

We are interested in understanding what sets the size and composition of these two wetting layers (one for each wall). These are the only clusters in the system since far from the walls the system is gaseous (the lower-density phase outside the layer is denoted "gas") with a density that is not sufficient to generate MIPS. Us-

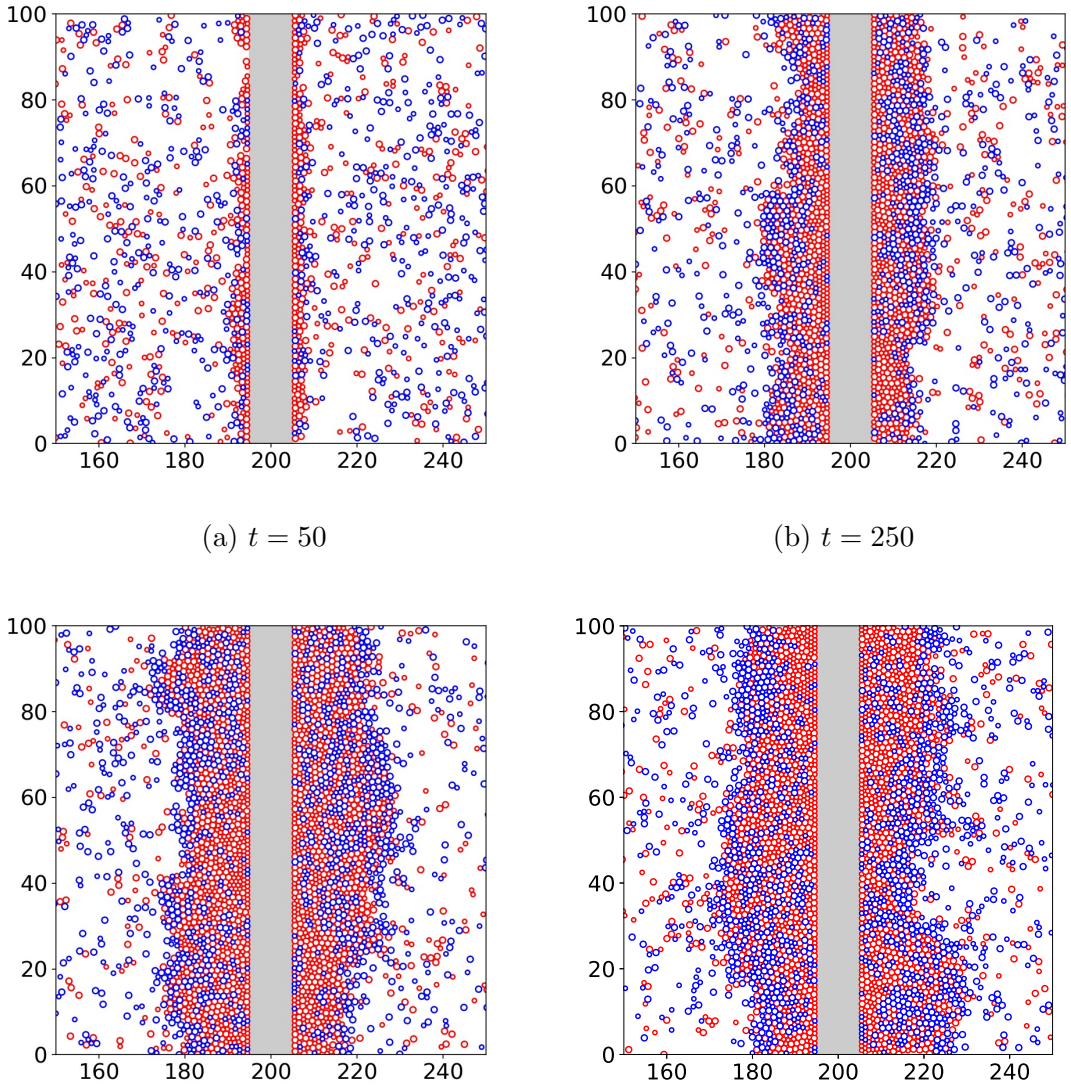

(a) $t = 50$ (b) $t = 250$

(c) $t = 500$ (d) $t = 1000$

Figure 3.2: Time evolution snapshots for $\delta = 0.5$ and $\phi = 0.18$. Only a portion of the simulated rectangular box is shown. Values for the other parameters are given in Chapter 2.

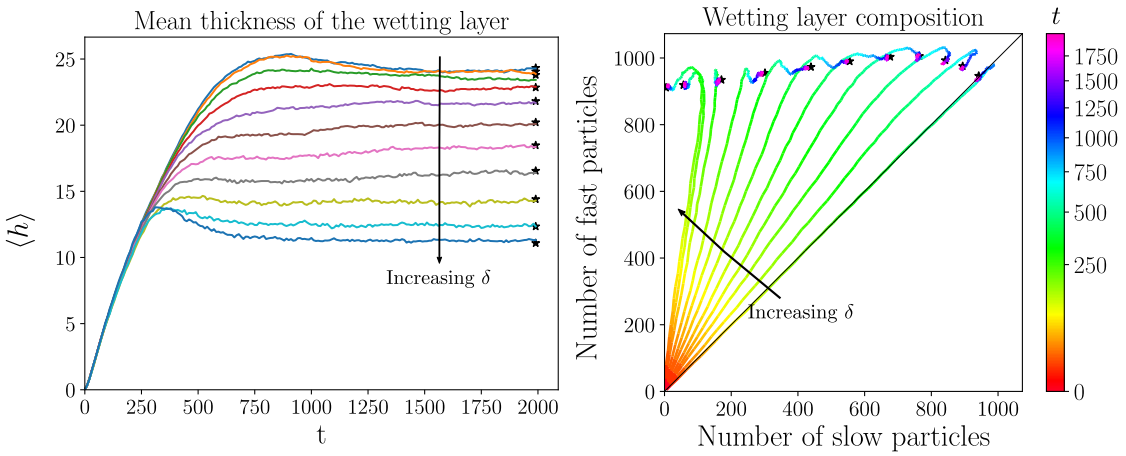

Figure 3.3: Left: Mean thickness of the wetting layer for various values of speed diversity δ (from 0 to 1 in steps of 0.1). We can see that increasing the diversity decreases the thickness of the layer. Right: Composition curve, i.e., evolution of the composition of the wetting layer for the same values of δ, measured in terms of the number of fast and slow particles in it. The diagonal corresponds to compositions with the same number of fast and slow particles. As δ increases, segregation emerges: the layer contains more fast particles than slow ones. For all values of δ, the behavior of the composition is separated into two stages, a fast dynamics and a slow one. In both plots, star symbols indicate results for the steady state ($t > 2000$). Here $\phi = 0.18$, corresponding to 6000 particles. The colorbar shows the time evolution and is scaled with a power law of exponent 1/2 to display evolution more clearly.

ing a standard graph approach based on the relative distance among particles and their respective radii, we found the two biggest connected components of particles in contact. Having identified the clusters, we used the layer particles located the farthest away from their respective wall to define the border of the wetting layer. We then calculated the mean distance of these borders to their corresponding wall and denoted it the mean thickness of the wetting layer $\langle h \rangle$.

Fig. 3.3(left) shows our simulation results for the mean thickness. The steady state values are shown with black stars through all this chapter. Far from the steady state, the wetting layer growth occurs at the same rate for all values of δ, in agreement with our theory below (see Section 3.3). For $0.3 \leq \delta \leq 0.8$, the size of the layer increases monotonically until it reaches its steady state value. For $\delta < 0.3$ and $\delta > 0.8$, on the other hand, the layer grows thicker than the stationary value, i.e., there is an overshoot, and then it relaxes by evaporating more particles than

absorbing. To complement and better understand this result, Fig. 3.3 (right) shows *composition curves* for various δ, i.e., the evolution of the wetting layer composition, measured in terms of the number of fast and slow particles in it. Each composition curve shows that the evolution occurs in two stages. First, there is a fast dynamics, where the ratio of the number of fast over slow particles is constant and different for each δ. Then, there is a slow dynamics, whose behavior depends qualitatively on δ as follows. In the range $0.3 \leq \delta < 0.8$, the slow dynamics shows additional aggregation of slow particles (the composition curves move to the right), which replace fast particles to balance emission and absorption rates (more below) while the total amount of particles in the layer is already stationary since the end of the fast dynamics process. This makes sense as equilibration of slow particles well inside the crowded layer (see the stationary state in Fig. 3.5 left) is expected to take longer than for fast particles. In the ranges $\delta < 0.3$ and $\delta > 0.8$, the slow dynamics of the wetting layer is characterized by evaporation (more than absorption) of both fast and slow particles. In these cases, during the fast transient dynamics the layer absorbed more particles in total than what is needed to reach the stationary state. For the active-passive mixture ($\delta = 1$), the number of passive particles in the wetting layer is zero in the steady state, meaning that the slow particles present in the layer during the fast dynamic are there because of a "wind" of active particles towards the wall, which traps slow particles until the layer relaxes in the slow dynamics, as shown in Movie 3.2. Such enhancement in the participation of passive particles in clustering phenomena as promoted by active ones has been observed in Ref. [46] in the context of MIPS.

The behavior shown in Fig. 3.3 can be explained as follows. Initially, there are no wetting layers, so the rate of evaporation of particles is zero and the rate of absorption is at its maximum. As time elapses, particles will start to accumulate, as shown in Fig. 3.1, and be able to escape after reorientation time $1/\eta$. If the layer has too many particles (more than the steady state size), the gas will have too few

particles, so the rate of absorption will decrease and eventually get lower than the evaporation rate, meaning that the layer will stop growing and start to lose particles until the rate of absorption increases again. This behavior will dump over time, until eventually the system relaxes to the NESS, as seen in Fig. 3.3 for $t > 1750$ for all of our mixtures.

Fig. 3.4 shows a spatiotemporal diagram of an orientation parameter used to study MIPS clusters in Ref. [63]. It is defined as $\alpha(x) = \langle -\hat{n}(x) \cdot \hat{\nu} \rangle$, where the unitary vector $\hat{n}$ is normal to the wall (outwards) and $\hat{\nu}$ is the self-propulsion direction, and averaged in y for each position x. Notice that it can independently capture the evolution of the mean wetting layer thickness shown in Fig. 3.3 (left), as drawn with a dashed black line in Fig. 3.4. Initially, orientations are random, so the number of particles pointing towards and away from the wall are the same, leading to $\alpha \approx 0$ everywhere. At later times, since particles have a persistent motion and take time to reorient, particles that were initially pointing away will be further from the wall and particles pointing inwards will accumulate near the wall. In this process, we observe a "cleanup" of particles pointing away from the wall. This cleaning "signal" will have a propagation velocity equal to the mean velocity in the x-axis for each particle type. Assuming random orientations, one obtains $\langle v_{\mathrm{f,s}} \rangle = \frac{2v_{\mathrm{f,s}}}{\pi}$ shown in Fig. 3.4 with dashed red and blue lines for fast and slow particles respectively. Again, there is an excellent agreement with the spatiotemporal orientation data from the simulations. Looking more closely at the interior of the wetting layer in Fig. 3.4, we notice that α takes more uniform values for the fast particles than for the slow ones. This is presumably due to the ability of fast particles to penetrate more as they are more persistent. This is a first sign that fast particles will accumulate closer to the wall and slow particles will be located nearer the interface, as further discussed below.

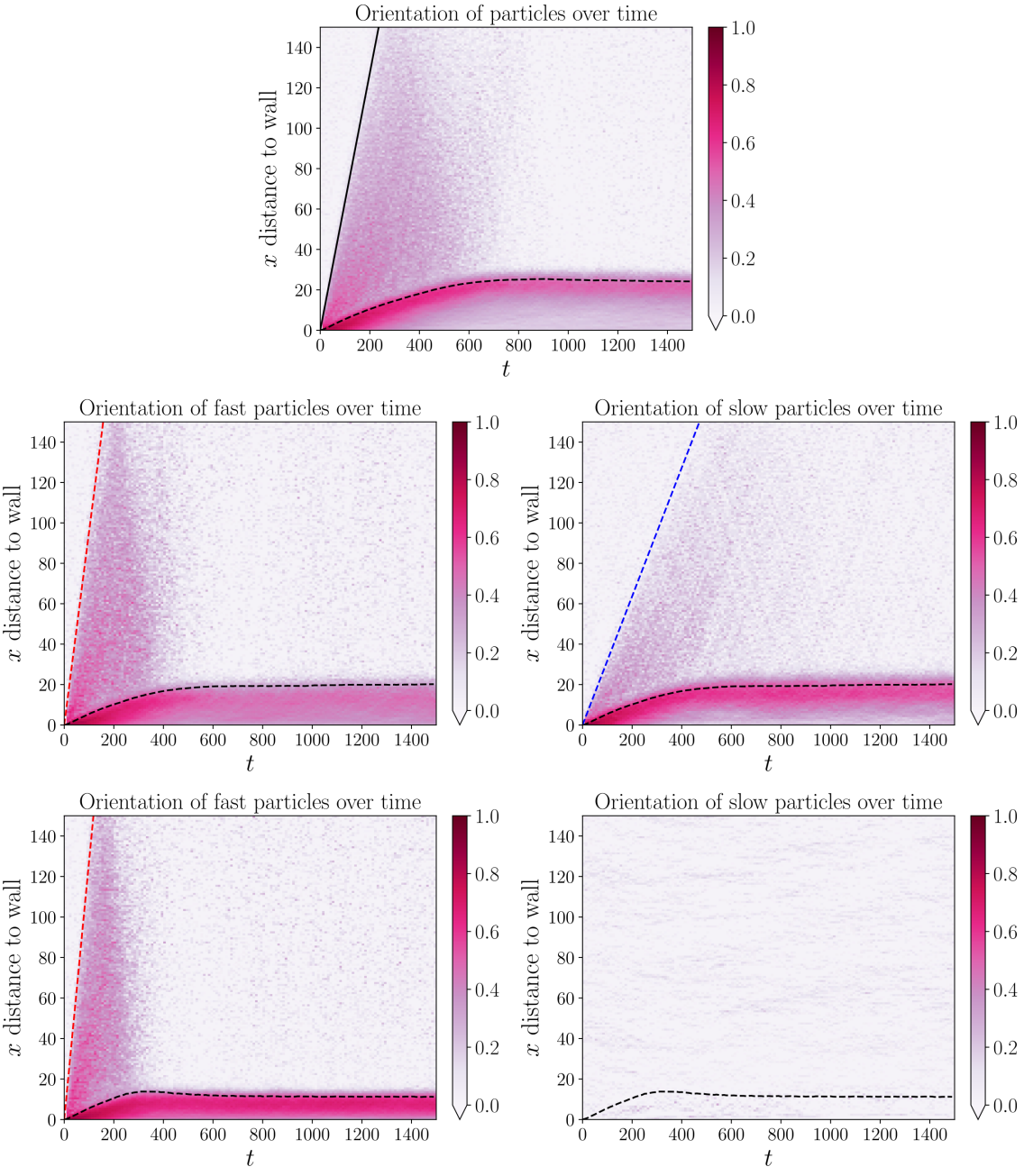

Figure 3.4: Spatiotemporal diagram of the orientation parameter $\alpha = \langle -\hat{n}(x) \cdot \hat{\nu} \rangle$, where the unitary vector $\hat{n}$ is normal to the wall (outwards) and $\hat{\nu}$ is the self-propulsion direction, for $\delta = 0$ (top row), $\delta = 0.5$ (middle row) and $\delta = 1$ (bottom row), with $\phi = 0.18$. The black dashed lines correspond to the mean thickness data shown in Fig. 3.3 (left). The dashed red and blue lines are the cleaning "signal" for fast and slow particles respectively. For $\delta = 0$ the cleaning "signal" curve is solid black.

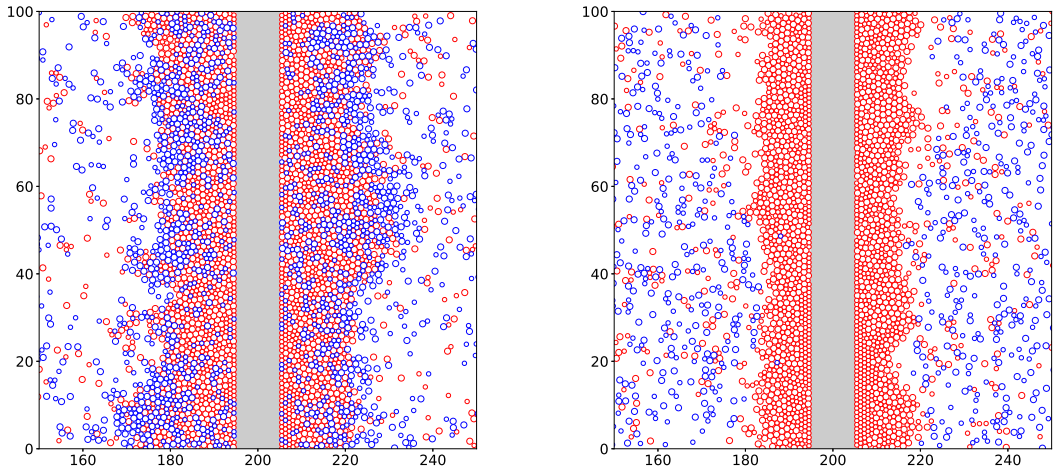

Figure 3.5: Snapshots of the system within the steady state for $\delta = 0.5$ (left) and $\delta = 1$ (right) and $\phi = 0.18$.

3.2 Stationary state

Once the wetting layer stops growing and the number of particles of each type fluctuates only weakly, we say that the system is within the NESS. The averaged NESS data shown in this section corresponds to $t > 5 \times 10^3$. Fig. 3.5 shows snapshots within the steady state for $\delta = 0.5$, where there are more fast particles near the wall whereas the slow ones are located near the interface. For $\delta = 1$, there are almost no slow particles in the wetting layer. To characterize this change of behavior we plot in Fig. 3.6 the concentration profiles $n_{\mathrm{f}}(x)$ and $n_{\mathrm{s}}(x)$ for the fast and slow particles respectively. They are defined as a local area packing fraction and are calculated by counting the number of particle centers in stripes parallel to the wall of width 1. These profiles provide information on where fast and slow particles accumulate. As shown in Fig. 3.5, fast particles tend to accumulate closer to the wall. This has two contributions: a kinetic one, which comes from the fact that fast particles are more likely to occupy newly available spaces first, and a dynamic one, which arises because faster particles can penetrate, i.e., open the way towards the wall by displacing other particles. On the other hand, slow particles tend to accumulate further from the

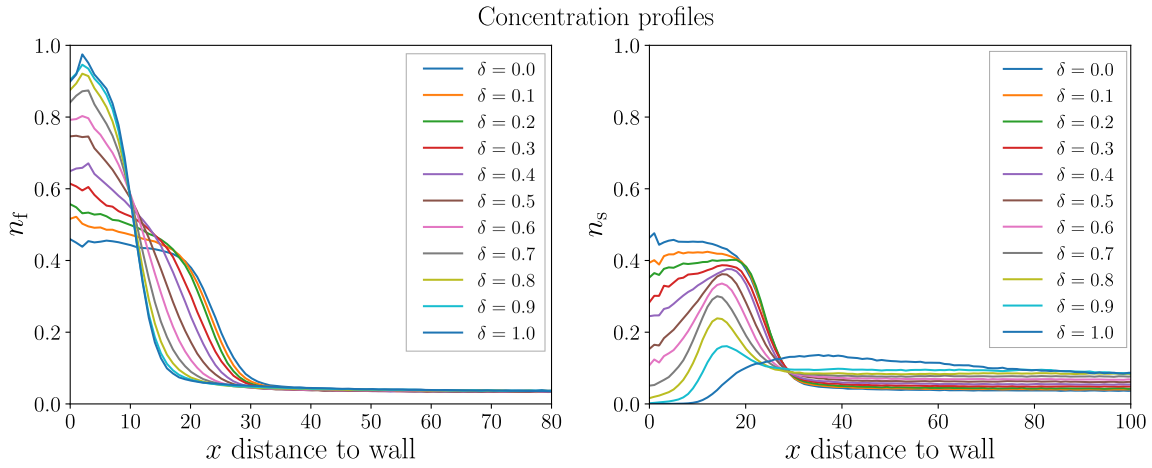

Figure 3.6: Concentration profiles within the steady state for fast (left) and slow (right) particles. Here $\phi = 0.18$.

wall. For $\delta \geq 0.3$, the slow-particle profile develops a local maximum: it becomes easier to accumulate over the layer of fast particles than near the wall. We also notice the presence of small oscillations in such concentration profiles near the walls. They do not correspond to poor-statistics effects. Instead, they can be attributed to the fact that, near the walls, particles accumulate in a series of stable one-particle layers, so that the concentration profile cannot be flat there.

To measure the global degree of spatial segregation, we calculate a segregation parameter that takes into account the overlapping between the concentration profiles [64], that is,

$$\zeta = 1 - \frac{\int n_s(\boldsymbol{r}) n_f(\boldsymbol{r}) dxdy}{\sqrt{\int n_s^2(\boldsymbol{r}) dxdy \int n_f^2(\boldsymbol{r}) dxdy}}. \tag{3.1}$$

As such, $\zeta = 1$ implies complete segregation and $\zeta = 0$ means complete mixing, which in turn occurs only if $n_s(\boldsymbol{r}) \propto n_f(\boldsymbol{r})$. Fig. 3.7 (left) shows that the degree of segregation increases with speed diversity, but complete segregation is never obtained, not even in the active-passive limit. One might think that this is because for $\delta = 1$ passive particles may remain trapped near the wetting interface even at long times due to active dragging. While this does occur, we will see below that on average almost all passive particles are eventually expelled from the wetting layer in this limit, with only a couple of them showing up at some time instants. The

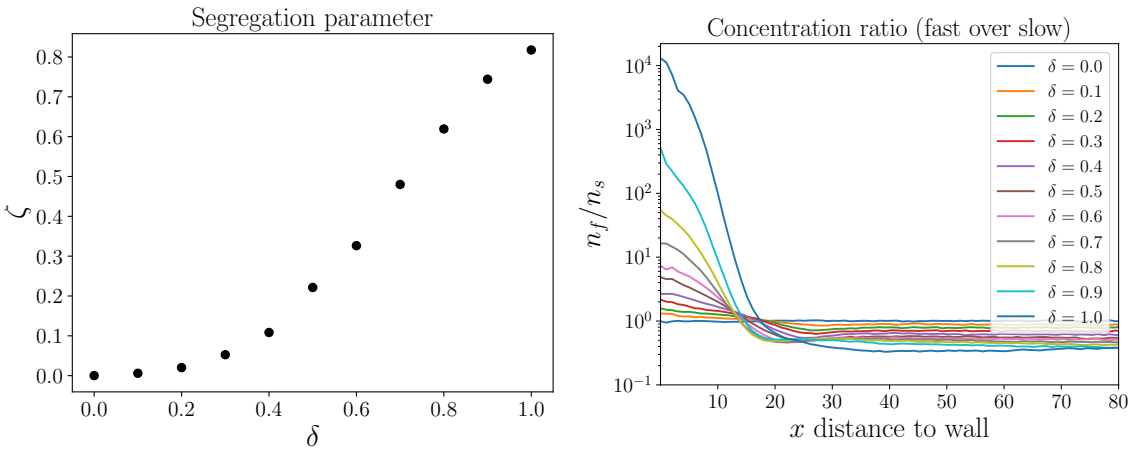

Figure 3.7: Segregation parameter (left) and concentration profiles ratio (fast over slow) within the steady state. Here $\phi = 0.18$.

more significant reason why complete segregation is not achieved is that there are fast particles in the bulk even for $\delta = 1$, i.e., the profiles do overlap. Fig. 3.7 (right) shows that near the wall the ratio between the fast and slow particles profiles increases one order of magnitude between $\delta = 0.8$ and $\delta = 0.9$, and then, since there are almost no slow particles in the wetting layer for $\delta = 1$, the ratio increases yet more than one order of magnitude between $\delta = 0.9$ and $\delta = 1$. This shows that the case $\delta = 0.9$ is not as close to an active-passive mixture ($\delta = 1$) as one might expect. This will be further discussed in Chapter 4.

Fig. 3.8 shows that the mean wetting layer thickness decreases with speed diversity. That is, systems that are more diverse in self-propulsion speeds form smaller wetting layers. This corroborates the behavior found for a one-dimensional lattice model of RTPs undergoing motility-induced clustering without wall facilitation [65]. The explanation is similar. Cluster (or wetting layer) sizes are ultimately set by the average time that an arbitrary particle takes to cross a gas region between clusters (compared with the reorientation time of the interface particles). That average time is the arithmetic average of the travel time for slow particles and the travel time for fast particles. This average is proportional to the inverse of the harmonic average of the fast and slow speeds, which increases with δ. If the average travel time is high,

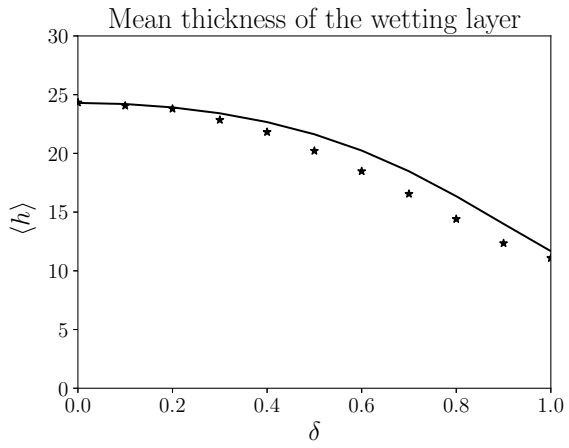

Figure 3.8: Mean thickness of wetting layer in the NESS for $\phi = 0.18$. The stars correspond to the simulation results and the solid line corresponds to the theory from Section 3.3.

interface particles can reorient and escape, thus leading to small wetting layers.

The stationary composition of the wetting layer is shown in Fig. 3.9, where $N_c^{(\mathrm{f/s})}$ correspond to the number of fast and slow particles in the wetting layer (detailed in Section 3.3). By increasing diversity, the number of fast particles is almost constant, with a only weakly non-monotonic behavior that peaks at intermediate values of δ. On the other hand, the amount of slow particles decreases strongly up to zero in the active-passive limit. As a result, the ratio of slow to fast particle number decreases to zero as well. To build additional insight into the stationary composition of the whole system, we divided it into rectangular boxes of dimensions 5×20 and counted the number of centers of fast and slow particles in each box. Then we divided this quantity by the area of the box to obtain the occupied area fraction. Fig. 3.10 shows the resulting 2D histogram of the local area fraction for each particle type. The histogram has two peaks, one corresponding to the composition of the wetting layer (high total area fraction, i.e., far from the plot origin) and another one to the composition in the gas (low total area fraction, i.e., near the plot origin). Between them one has the compositions found by crossing the interface between the dense and dilute phases. For the relatively small value $\delta = 0.3$, the dense phase is close to the complete mixing and the interface and gas are almost totally well mixed.

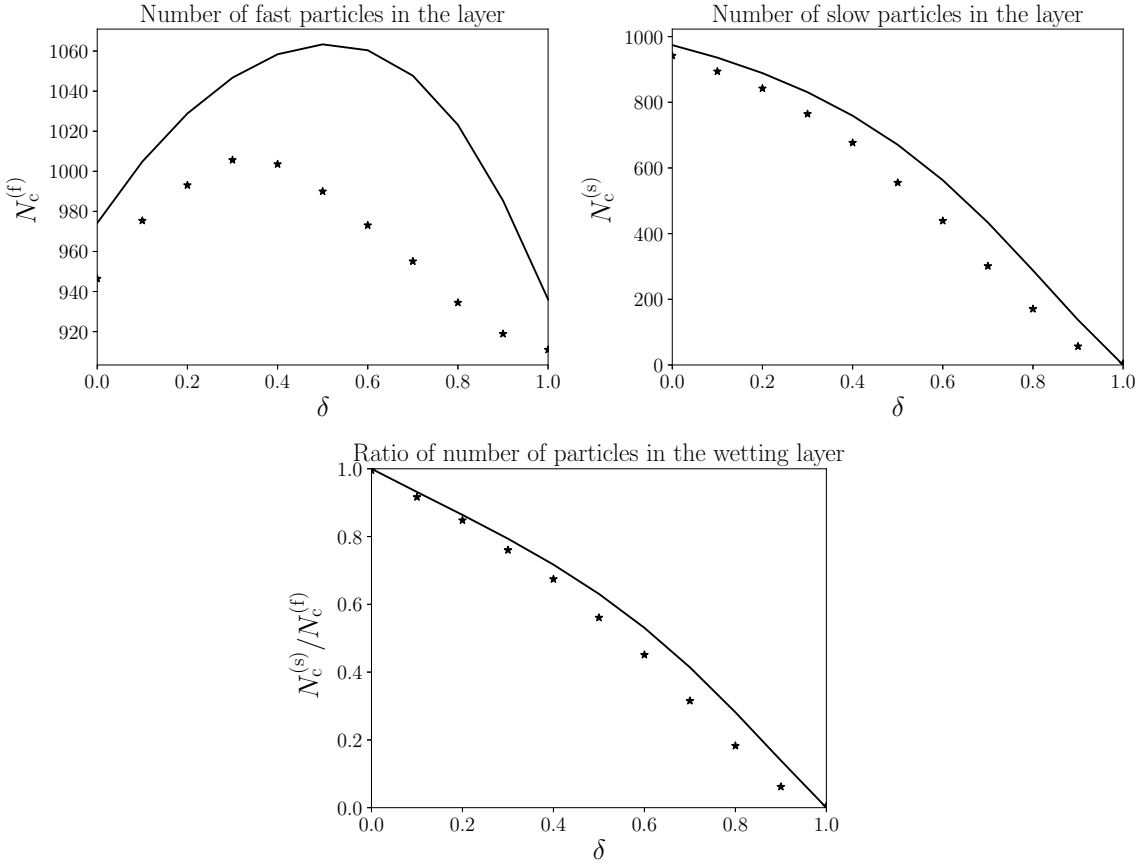

Figure 3.9: Number of fast (left) and slow particles (right) in the layer as a function of δ. The ratio between the number of fast and slow particles in the layer is at the bottom row. The solid lines are the theoretical prediction (Section 3.3) and the stars show the simulation results.

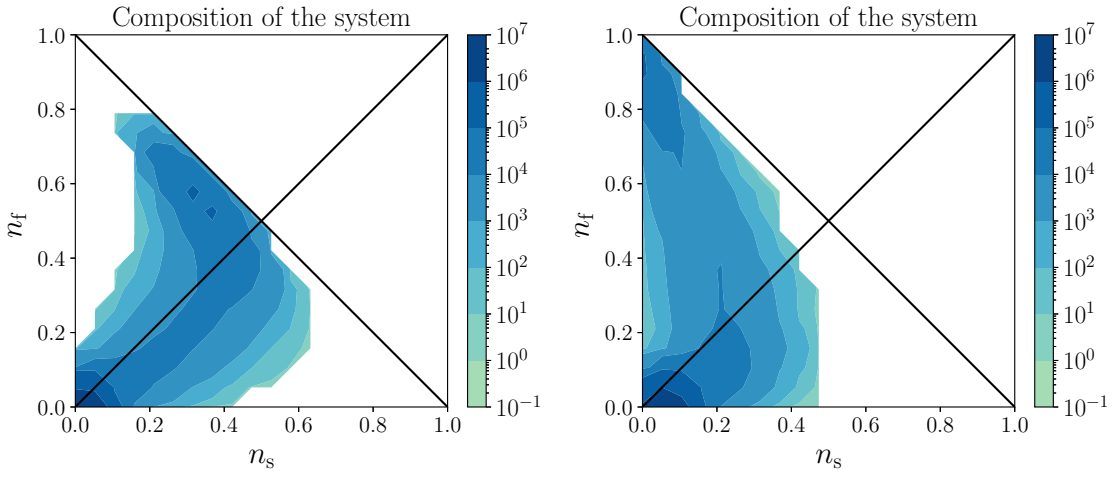

Figure 3.10: Composition histogram of the whole system for $\delta = 0.3$ (left) and $\delta = 0.8$ (right) within the NESS. It is a contour plot obtained from histograms of the compositions for various configurations within the NESS. The diagonal line that starts at the origin indicates compositions with the same number of fast and slow particles, whereas the perpendicular diagonal indicates the maximum area density. Contour levels are spaced logarithmically.

This behavior changes for $\delta = 0.8$, where the dense phase moves towards the upper-left corner and thus only a few slow particles are present in the dense phase (high segregation). Also, most locations near the interface now have compositions that are far from complete mixing.

3.3 Kinetic Theory

To further develop our insights, we apply the kinetic approach by Redner *et al.* [15] to wetting. After presenting its derivation (including the details omitted in Ref. [15]), we generalize it to mixtures.

Consider a monodisperse system of active Brownian particles with self-propulsion speed v and rotational diffusivity η. In the steady state, let us assume that a single macroscopic motility-induced cluster forms. Moreover, consider it to be close packed and large enough so that its interface can be treated as flat. Without lack of generality, we take the dense phase to be on the right and a dilute gas of non-interacting particles on the left. The flat interface is located along the y-axis in

between the two phases. The gas particles travel at the self-propulsion speed v with an angle θ with the x-axis. Kinetic equilibrium is achieved when $k_{\rm in} = k_{\rm out}$, where $k_{\rm in}$ ($k_{\rm out}$) is the rate of absorption (emission) of particles per unit length, i.e., the flux. For $k_{\rm in}$, one can write

$$k_{\rm in} = \rho_{\rm g} \int_{-\pi/2}^{\pi/2} \frac{1}{2\pi} v \cos\theta d\theta = \frac{\rho_{\rm g} v}{\pi}, \tag{3.2}$$

where $\rho_{\rm g}$ is the gas number density, i.e., particles per area. The angle integral takes into account only those particles in condition to be absorbed, that is, those moving from left to right. Since particles escape from the cluster once $\theta = \pm\pi/2$. The outgoing flux $k_{\rm out}$ can be calculated by solving the diffusion equation in angular space for P, the time-dependent distribution of orientations for the particles at the interface, i.e.,

$$\partial_t P(\theta, t) = \eta \partial_\theta^2 P(\theta, t), \tag{3.3}$$

with absorbing boundaries at $\pm\pi/2$ and initial condition given by the distribution of incident particles, that is, $P(\pm\pi/2, t) = 0$ and $P(\theta, 0) = \cos\theta/2$. The corresponding solution is

$$P(\theta, t) = \frac{e^{-\eta t}\cos\theta}{2}, \tag{3.4}$$

For particles of diameter σ, one can write

$$k_{\rm out} \equiv -\frac{\dot{N}_{\rm interface}}{\sigma N_{\rm interface}}, \tag{3.5}$$

where $N_{\rm interface}$ is the number of particles at the interface and the dot represents the time derivative. Considering only the above, one would obtain

$$k_{\rm out} = -\frac{\partial_t \int_{-\pi/2}^{\pi/2} P(\theta, t) d\theta}{\sigma \int_{-\pi/2}^{\pi/2} P(\theta, t) d\theta} = \frac{\eta}{\sigma} \tag{3.6}$$

However, each time a particle escapes from the interface towards the gas, other particles pointing towards the gas will follow it in an avalanche-like effect. The

average number of particles leaving the cluster per escape event is denoted κ and is treated as a fitting parameter (Ref. [15] found that $\kappa \approx 4.5$ works well for all studied self-propulsion speeds and global concentrations). Thus, one corrects k_{out} by multiplying it by κ. The final balance equation is

$$\frac{\rho_{\text{g}} v}{\pi} = \frac{\kappa \eta}{\sigma}. \tag{3.7}$$

Knowing the gas density, one can now proceed to obtain the number of particles in the dense phase and thus its size.

Additional equations are needed. First, there is conservation of area, $A = A_{\text{g}} + A_{\text{c}}$, where A_{g} and A_{c}, where the subindices c and g refer to the cluster (or wetting layer) and the gas respectively. There is also particle conservation, $N = N_{\text{c}} + N_{\text{g}}$, where N denotes number of particles. This can be rewritten as $\rho A = \rho_{\text{g}} A_{\text{g}} + \rho_{\text{c}} A_{\text{c}}$, considering the number densities multiplied by the area of each corresponding region. We now use that $\phi_{\text{c}} = \rho_{\text{c}} a_{\text{p}}$, where $a_{\text{p}} = \pi(\sigma/2)^2$ is the particle's area, so that for the global and cluster area fraction we have $\phi = \rho a_{\text{p}}$ and $\phi_{\text{c}} = \frac{\pi}{2\sqrt{3}}$, where we assume that the cluster is close packed. Using these equations and the equilibrium condition $k_{\text{in}} = k_{\text{out}}$, we close the system of equations. Finally, applying this to wetting via $h \equiv A_{\text{c}}/L_y$ gives the wetting layer thickness.

We now generalize to speed-diverse mixtures. Detailed balance per particle type is assumed. A somewhat similar derivation has been discussed in Ref. [46] in the context of MIPS (no walls) for active-active mixtures at global ratios other than 50-50%, where the authors considered the approximation that the emission rate for each type is proportional to the *global* fraction of that type. Since we know that the system segregates fast and slow particles, and our system has the same number of each type, we go beyond that approximation and say instead that the emission rate of each type should be proportional to the ratio of particles of the same type in the *wetting layer* (not globally) divided by the total number of particles in it. That is,

we now have

$$k_{\text{out}}^{(\text{f})} = \frac{\kappa\eta}{\bar{\sigma}} \frac{N_{\text{c}}^{(\text{f})}}{N_{\text{c}}^{(\text{f})} + N_{\text{c}}^{(\text{s})}} \tag{3.8}$$

$$k_{\text{out}}^{(\text{s})} = \frac{\kappa\eta}{\bar{\sigma}} \frac{N_{\text{c}}^{(\text{s})}}{N_{\text{c}}^{(\text{f})} + N_{\text{c}}^{(\text{s})}} \tag{3.9}$$

where $\bar{\sigma} = 1.2d_0$ is the mean particle diameter.

The absorption rates are according to the corresponding velocities: (3.10). Notice that in the dilute gas regime studied here (low and intermediate global ϕ) one does not need to worry about the interactions between types in the gas and thus

$$k_{\text{in}}^{(\text{f/s})} = \frac{v_{\text{f/s}} \rho_{\text{g}}^{(\text{f/s})}}{\pi} \tag{3.10}$$

In order to close the equations, we use particle conservation per type, $A\rho^{(\text{f/s})} = A_{\text{c}}\rho_{\text{c}}^{(\text{f/s})} + A_{\text{g}}\rho_{\text{g}}^{(\text{f/s})}$ and $\rho_g = \rho_{\text{g}}^{(\text{s})} + \rho_{\text{g}}^{(\text{f})}$, leading to a total of 7 equations and 7 unknowns.

As can be seen in Section 3.2, the quantitative agreement between this theory and the simulations is excellent, with numerical deviations being smaller than 5%. The only fitted parameter across all data and physical parameters is $\kappa = 4.7$. Qualitative non-monotonic behaviors are also captured. For the number of fast particles in Fig. 3.9, good agreement is also obtained, but the intense zoom-in makes it look less accurate.

We also used this approach to predict the evolution of the system. We write two master equations for the number of particles in the layer based on the difference between the rates of emission and absorption per unit length for each particle type, i.e.,

$$\frac{dN_{\text{c}}^{(\text{f/s})}}{dt} = \left(k_{\text{in}}^{(\text{f/s})} - k_{\text{out}}^{(\text{f/s})} \right) L_y. \tag{3.11}$$

Fig. 3.11 shows the theoretical results for the wetting layer thickness as a function of time, for which we used a conventional Euler scheme to solve (Eq. 3.11). Our dynamical theory reaches the steady state at somewhat similar times but in the simulations this occurs after an overshoot which is not captured by the theory, presumably because it does not consider dragging or "wind".

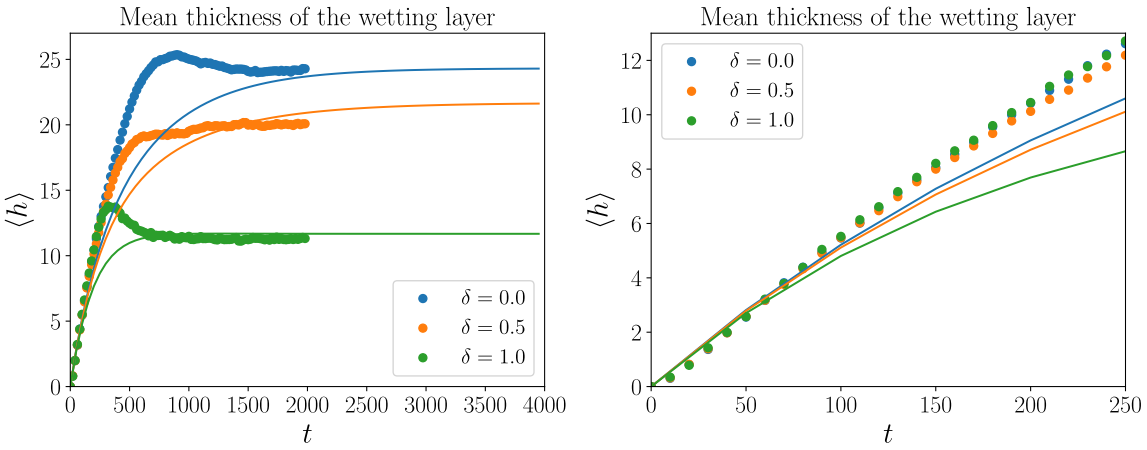

Figure 3.11: Evolution of the mean thickness of the wetting layer for three values of δ. Solid lines correspond to the numerical solution of Eq. (3.11) whereas the points are the simulation data. Left: Complete evolution. Right: Early-time data.

Chapter 4

Active mixtures interacting with asymmetric obstacles

In this chapter, we analyze the behavior of mixtures of active particles in the presence of an array of half-disk shaped obstacles. We start by reviewing the wetting behavior of active mixtures, but now on the curved and flat obstacle walls rather than on infinite flat walls. In doing so, we calculate concentration profiles and the global segregation parameter and compare them with the ones obtained in the previous chapter. Next, we study the effects of speed diversity on the stationary rectification currents that arise due to the obstacle's shape. We also observe the appearance of two pairs of vortices in the corners of the obstacle, which complement the explanation given in Ref. [33] for the rectification currents by noticing how particles move over the flat side.

4.1 Wetting and segregation

Movie 4.1 shows the dynamics between the initial state and the stationary state for $\phi = 0.26$ and $\delta = 0.8$. Snapshots of the initial and stationary states are shown in Fig. 4.1 for the monodisperse (i.e., one-component $\delta = 0$) case. After particles quickly accumulate around the obstacle, the average thickness of the wetting layer stabilizes once the concentration of the "gas" (i.e, outside the layer) becomes sufficiently low that absorption and emission rates for the layer are equal. Because available spaces are more likely to be occupied by the faster particles (as they arrive

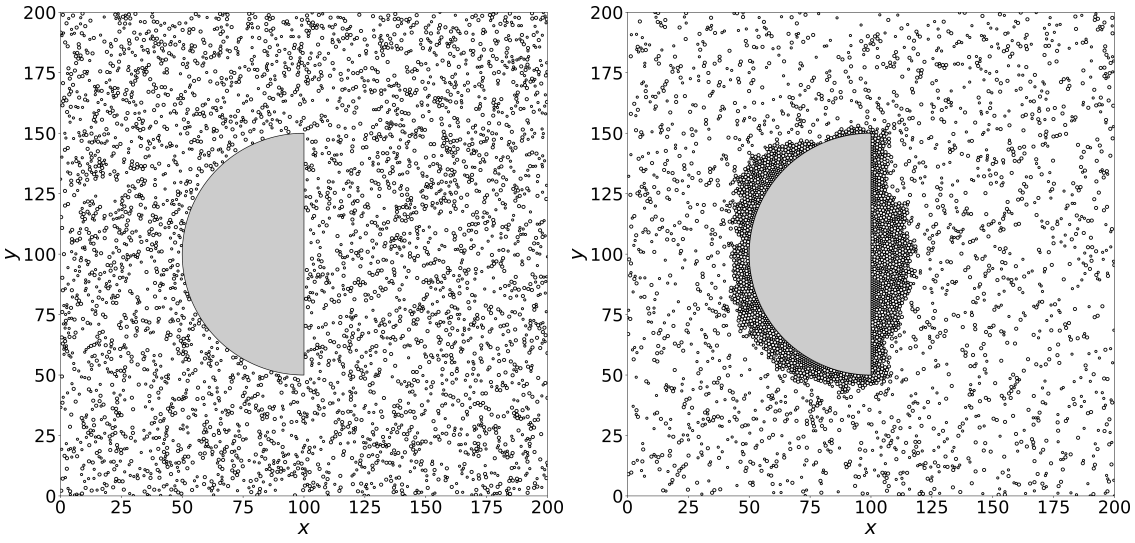

(a) $t = 1$ (b) $t = 8000$

Figure 4.1: Snapshots of the system for $\delta = 0$ (monodisperse case) and $\phi = 0.13$. Left: initial configuration. Right: configuration within the steady state.

there typically before the slower ones), segregation emerges. For larger area fractions, the wetting layer increases in size, as shown in Fig. 4.2 for $\phi = 0.26$. In all cases studied below ($\phi = 0.08$, 0.13, and 0.26 for various values of δ), the stationary gas concentration is sufficiently low such that no stationary clusters appear in the gas. That is, the residual gas density after the wetting layer has been formed is smaller than the necessary to produce MIPS [14]. Also, in the transient regime, the condensation by heterogeneous nucleation on the obstacle is faster than an eventual MIPS. Hence, the only condensed phase in the system is the wetting layer on the obstacle. Movies 4.2 and 4.3 show, respectively, the transient and the steady state for $\phi = 0.26$ with $\delta = 0.8$.

Due to crowding, the dynamics inside the wetting layer is much slower than that in the gas. Movie 4.1 also shows that the interface between the wetting layer and the gas fluctuates strongly. Presumably, this is a consequence of active capillary-like effects [66, 67] enhanced by the fact that particles can escape from the cluster not only by rotational diffusion but also by reaching the end of the obstacle wall.

Fig. 4.3 shows the stationary concentration fields for the total, "slow", and "fast"

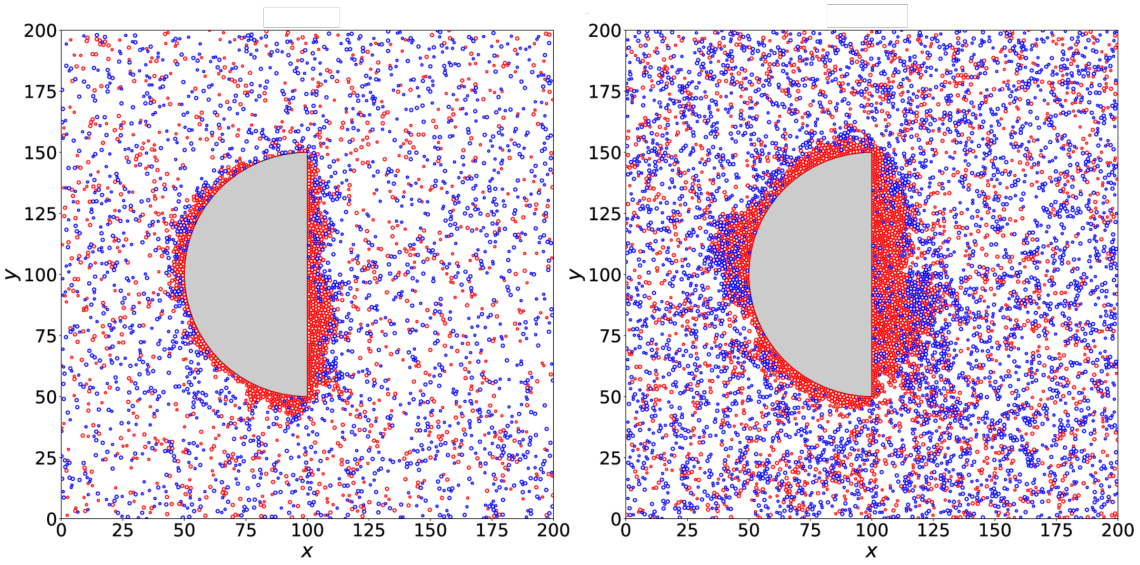

Figure 4.2: Snapshots of the system for $\delta = 0.8$, with the faster particles in red and the slower ones in blue. The gray area corresponds to the obstacle. Configurations within the steady state for $\phi = 0.13$ (left) and $\phi = 0.26$ (right).

particles concentrations, denoted respectively by $n(\boldsymbol{r})$, $n_{\mathrm{s}}(\boldsymbol{r})$, and $n_{\mathrm{f}}(\boldsymbol{r})$, for selected values of ϕ and δ. They are defined similarly to the concentration profiles for the wall but are calculated locally using coarse-graining square boxes of side 2.5. We counted the number of particle centers in each box, multiplied by the area of the corresponding particle, and then divided the result by the area of the coarse-graining box. For boxes that include a fraction of the obstacle, the available area was calculated using standard Monte Carlo integration.

Fig. 4.3 (top row) shows the monodisperse ($\delta = 0$) scenario studied in Ref. [33]. The stationary accumulation is more pronounced for higher ϕ and decays smoothly towards the gas. For $\delta > 0$, we observe that $n_{\mathrm{s}}(\boldsymbol{r})$ and $n_{\mathrm{f}}(\boldsymbol{r})$ are significantly different from each other as the faster particles once again dominate the occupation closer to the obstacle, whereas the slower particles accumulate less sharply. Concentration profiles were obtained by averaging the concentration fields along the direction parallel to each wall. Fig. 4.4 (left column) shows concentration profiles of the slow particles for both sides and several values of δ. For the curved side, the concentration is plotted against the radial distance to the wall. In this case, a peak located

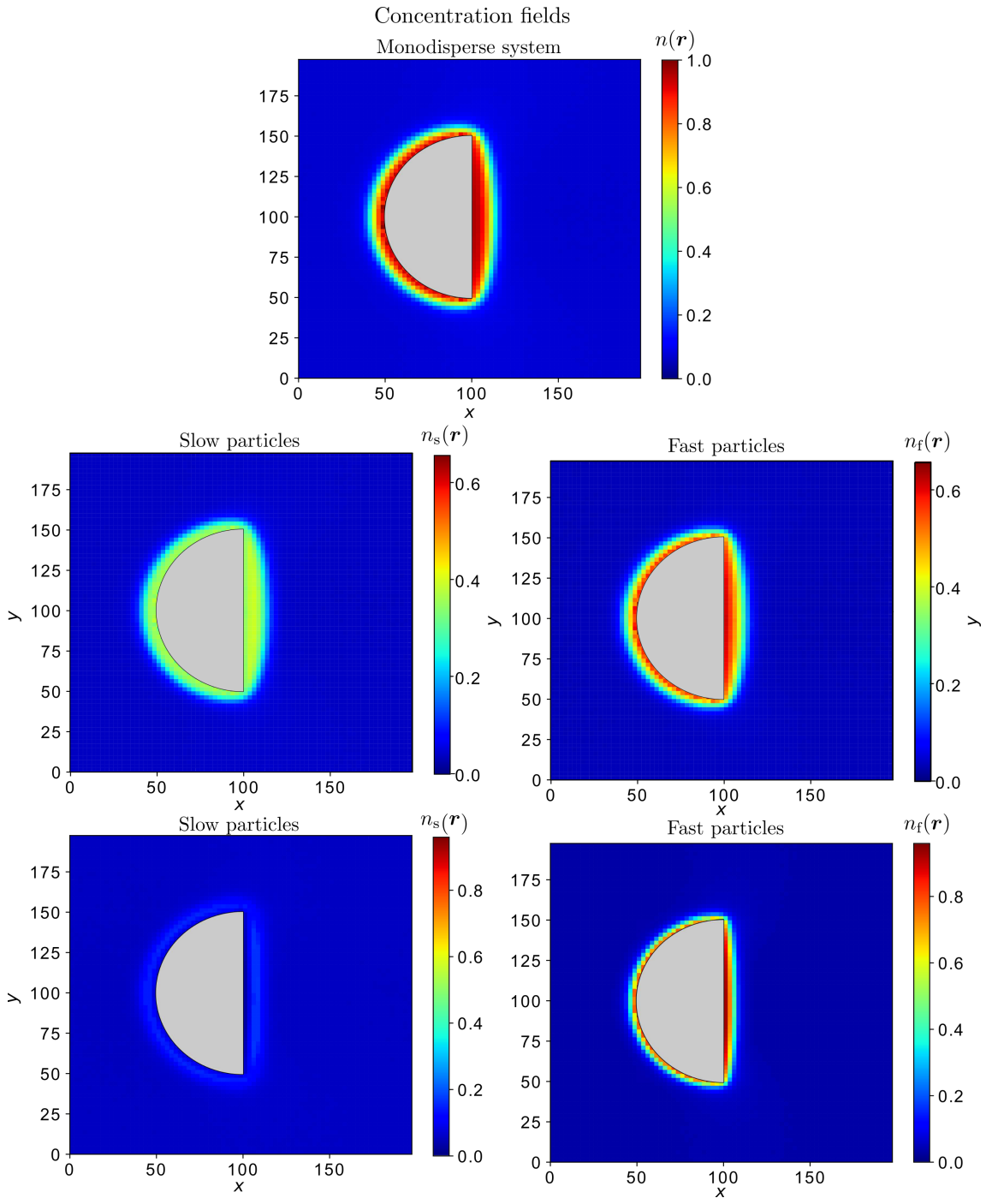

Figure 4.3: Concentration fields for $\delta = 0$ (top row) and, per particle type, for $\delta = 0.2$ (middle row) and $\delta = 0.8$ (bottom row). Here $\phi = 0.13$.

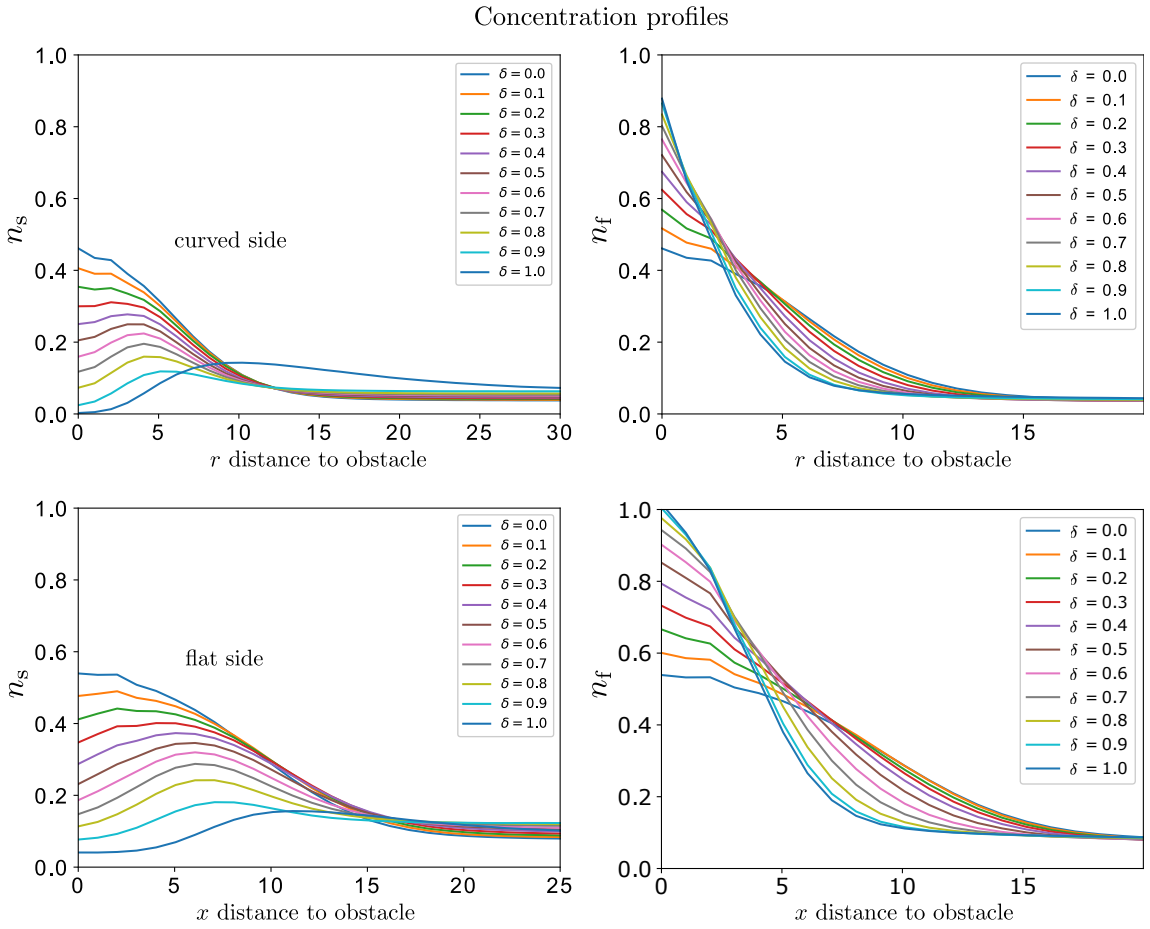

Figure 4.4: Stationary concentration profiles of slow (left) and fast (right) particles for various δ and $\phi = 0.13$ and for the curved (top) and the flat (bottom) sides.

further away from the obstacle is observed for $\delta \geq 0.4$. As before, this transition occurs when the slower particles become sufficiently slow that they accumulate more easily on the boundary of the "layer" of faster particles than closer to the obstacle wall. Notice that the peak is less pronounced on the curved side. The concentration of faster particles decays monotonically towards the gas irrespective of δ, just like in the flat-wall case of Chapter 3, for both the curved and flat sides, as shown in Fig. 4.4 (right column). This accumulation of fast particles can be explained with the same reasoning described in Chapter 3.

To measure the degree of spatial segregation, we calculated the segregation parameter (Eq. 3.1). Fig. 4.5 shows that the degree of segregation increases with speed diversity, but complete segregation is again not obtained, not even in the

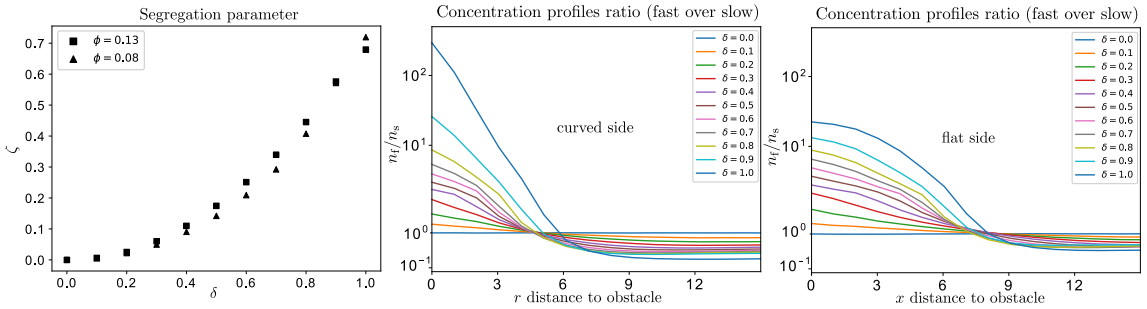

Figure 4.5: Segregation parameter for two values of ϕ (left) and concentration profiles ratio (fast over slow) for the curved (center) and the flat (right) side. Here $\phi = 0.13$.

passive-active limit. In this case too, this is because profiles also overlap and also some passive particles remain trapped inside the wetting layer by the active ones. Furthermore, Fig. 4.5 (left) shows that the degree of segregation in the low global concentration limit is almost independent of ϕ. Just like in the flat-wall case of Chapter 3, we calculated the ratio between the concentration profiles n_f/n_s. This is shown in Fig. 4.5 for the curved and the flat sides, providing information on the local proportions between the two particle types in the different parts of the system. For $\delta = 1$, there are almost no passive particles near the wall and the curved side concentration ratio is more than one order of magnitude bigger than for $\delta = 0.9$. Again, this shows that the case $\delta = 0.9$ is not as close to a active-passive mixture as one might expect. In fact, Figs. 3.6 and 4.4 show a significant difference in the behavior of the concentration profile between $\delta = 0.9$ and $\delta = 1$. This can be understood by noticing that for $\delta = 0.9$ the slow particles persistence length $v_s/\eta = v_0(1-\delta)/\eta = 20$ is still comparable to other relevant length scales such as the wetting layer thickness, the obstacle size, and the system size. We also notice that there is more segregation on the curved side than on the flat side as particles are less capable to penetrate and settle inside that layer. For slow particles, such "expulsion" effect becomes more pronounced. It is almost impossible for a particle with weak self-propulsion to remain near the wetting interface without being wiped out into the gas by the rectification "wind" (see Section 3.3 above). Conversely, particles on the flat side can accumulate closer to the wall since the particle current

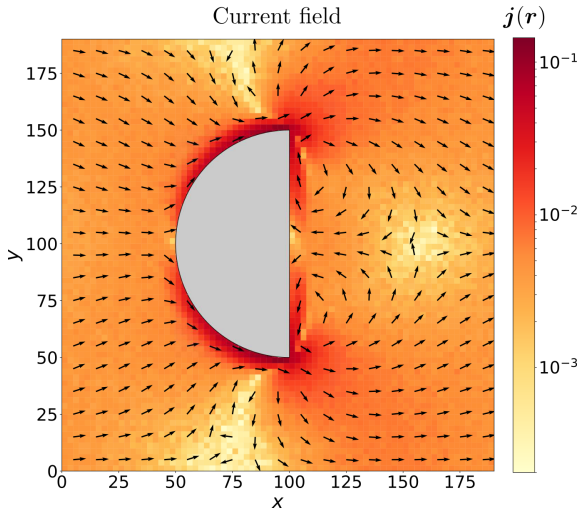

Figure 4.6: Total stationary current field for $\phi = 0.13$ and $\delta = 0.8$. All arrows have the same size and only indicate the direction of the current $\boldsymbol{j}$. The magnitude of $\boldsymbol{j}$ is given via the color legend.

on the flat side near the interface is not sufficient to wipe them out. This can be confirmed by looking once again at the passive particles profile ($\delta = 1$) in Fig. 4.4, where the concentration near the wall is practically zero on the curved side but not so on the flat side.

4.2 Rectification and vorticity

The asymmetric shape of the obstacle implies that particles travelling from the curved to the flat side will spend less time to overcome it than those in the opposite direction. In the monodisperse case ($\delta = 0$), a rectification current arises in the stationary state [33]. We now focus on the behavior for $\delta > 0$.

Fig. 4.6 shows the total stationary current (vector) field $\boldsymbol{j}(\boldsymbol{r}) \equiv n(\boldsymbol{r})\,\boldsymbol{v}(\boldsymbol{r})$, where $\boldsymbol{v}(\boldsymbol{r})$ is the actual velocity field (not the self-propulsion velocity field). Global rectification along the $+x$ direction is indicated by the fact that most current arrows point to the right or have a large $+x$ component. Particles slide on the curved side towards the right and are subject to higher current than in the gas. The highest local current is observed near the corners. For the flat side, the local current is in the opposite direction, i.e., the $-x$ direction (reflecting the appearance of vortices,

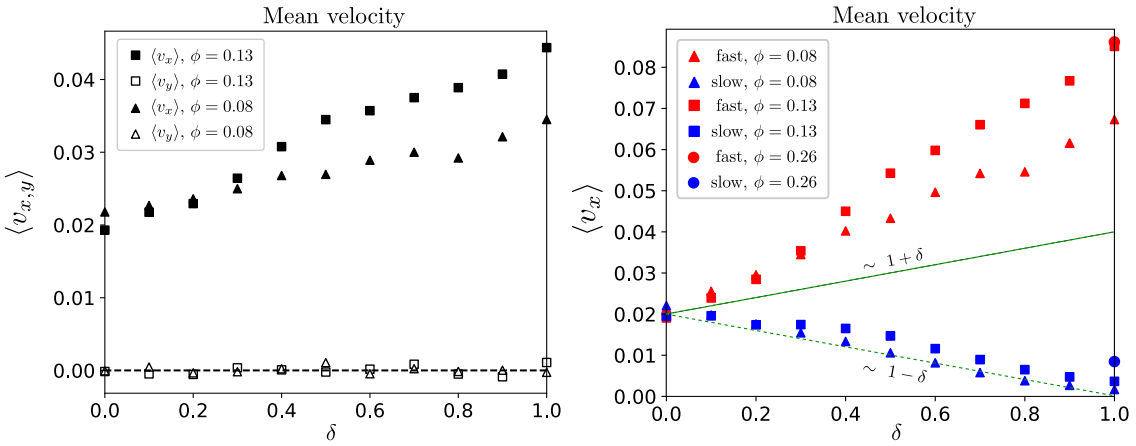

Figure 4.7: Stationary mean (actual) velocity averaged over particles and realizations as a function of δ for $\phi = 0.08$ and $\phi = 0.13$. Total mean velocity in x and in y (left). Mean velocity in x for slow and for fast particles (right). The case $\phi = 0.26$ has been included only for $\delta = 1$, avoiding an overcrowding of the figure. The dashed lines present the naive δ-dependence for the mean velocity of the fast and slow particles.

as discussed below), but near the obstacle, it is constrained to the y-axis only. Far from the obstacle, the current field changes to the $+x$ direction again.

To investigate how rectification is affected by speed diversity, we show in Fig. 4.7 (left) the mean of the actual velocity in x, $\langle v_x \rangle$, averaged over particles and time instants within the steady state, as a function of δ. As a control, we also show that $\langle v_y \rangle$ is essentially zero, as expected. More importantly, $\langle v_x \rangle$ increases with δ, indicating an *amplification* of rectification currents that are induced solely by speed diversity (remember that each type corresponds to 50% of all particles and the system-average self-propulsion speed does not change with δ). By looking at $\langle v_x \rangle$ for each particle type in Fig. 4.7 (right), we see that, indeed, as δ increases, the faster particles undergo a rectification *increase* which is larger than the rectification *decrease* of the slower particles, even though their self-propulsion speeds were varied by the same amounts, in magnitude. Indeed, the average speed of fast particles is larger than the naive dependence proportional to $1+\delta$, a manifestation of significant interaction effects. The slow particles for low ϕ do follow the naive dependence proportional to $1 - \delta$, but as the density increases interactions take over, and their rectified velocity increases.

This rectification amplification induced by speed diversity can be understood as follows. First, $\langle v_x \rangle(\delta)$ must be an even function of δ since $\delta \to -\delta$ just relabels particle types and thus should have no physical consequence. Now, consider the monodisperse case of Ref. [33]. Fig. 3a therein suggests that the rectification current obeys $\langle v_x \rangle \approx \exp(-\eta d_0/v_0)$, where we remind that η is the rotational diffusion coefficient and we incorporated the self-propulsion speed v_0 and the particles' diameter by dimensional analysis. This makes sense: by increasing the active speed v_0, activity-induced rectification ought to increase as well.

We now assume that the *qualitative* behavior of $\langle v_x \rangle(\delta)$ can be obtained simply from an arithmetic average between $\exp(-\eta d_0/v_\mathrm{s})$ and $\exp(-\eta d_0/v_\mathrm{f})$ (On the other hand, the *quantitative* behavior should require a more complicated analysis, as indicated, for example, by the δ-dependence of motility-induced cluster sizes in a system of slow and fast RTPs studied in Ref. [65].) Expanding in δ, indeed no linear δ dependence survives, as anticipated. Also, for sufficiently high η, $\langle v_x \rangle(\delta)$ indeed increases with δ as observed numerically. (The same qualitative analytical examination indicates that a transition for much lower η *might* exist in the simulations, through which $\langle v_x \rangle(\delta)$ would become a decreasing function of δ. That is beyond our scope because the corresponding persistent lengths would be extremely large.)

Furthermore, Fig. 4.7 (right) shows that $\langle v_x \rangle$ for the slower particles does not vanish completely at the active-passive limit $\delta = 1$. The passive particles continue to contribute positively to the total $\langle v_x \rangle$. Such behavior where the motion of passive particles is "enhanced" by active ones has been previously reported in the context of motility-induced phase separation: the presence of active particles induces *clustering* for the passive ones [44, 46, 68], as found also in Chapter 3. Here what we find is that the active particles induce a finite degree of *rectification* for the passive ones, which increases with ϕ.

Revisiting the current field in the active-active mixture case, we notice that the flat side has a non-vanishing total local current moving away from the obstacle center

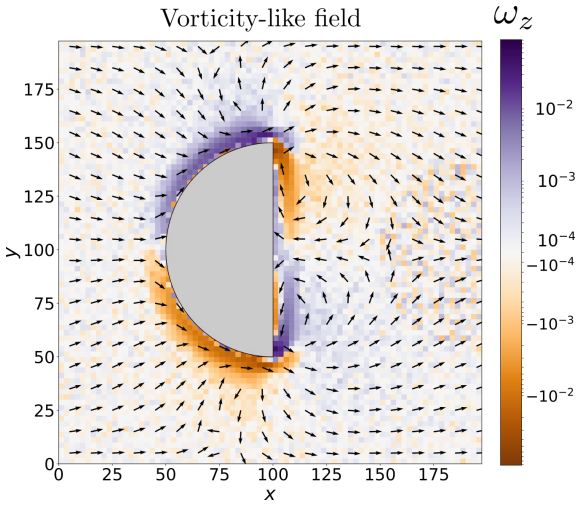

Figure 4.8: Vorticity-like field defined by the z-component of $\boldsymbol{\omega}(\boldsymbol{r}) \equiv \nabla \times \boldsymbol{j}(\boldsymbol{r})$, i.e., ω_z, for $\delta = 0.7$ and $\phi = 0.13$. The color scheme is shown on the left in symmetric logarithmic scale with positive values indicating counter-clockwise rotation and clockwise for the negative values. The arrows show the total particle current field.

along the y-axis. This behavior is connected to the appearance of vortices. We define

$$\boldsymbol{\omega}(\boldsymbol{r}) \equiv \nabla \times \boldsymbol{j}(\boldsymbol{r}) \tag{4.1}$$

as a vorticity-like field (not exactly the vorticity since it is the curl of the current field, not of the velocity field) and plot its z component in Fig. 4.8. We observe that one pair of vortices is formed around each obstacle corner. The vortices strengthen with δ with no qualitative change.

For each pair, one of the vortices is produced by the particles that slide on the curved side and the other by those that slide on the flat side. As a consequence, velocities become reoriented, thus generating the corresponding vortices. To see how vorticity changes with speed diversity, Fig. 4.9 shows the global vorticity magnitude, defined as $\Omega \equiv \int \omega(\boldsymbol{r})\, dx\, dy$, where we keep the signs in ω_z. The intensity of the vorticity also increases with δ: the particles that participate more in the vortices are those close to the obstacle and, as discussed above, these correspond to the faster particles.

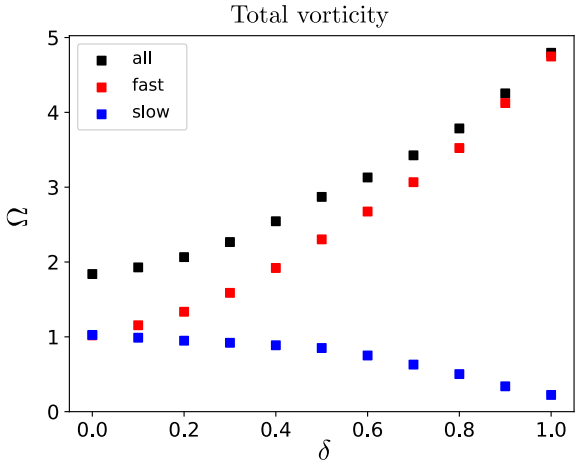

Figure 4.9: Added vorticity as a function of the δ for $\phi = 0.13$. The partial vorticities, for fast and slow particles, are obtained from the partial current fields $\boldsymbol{j}_{\mathrm{f/s}}(\boldsymbol{r}) \equiv n_{\mathrm{f/s}}(\boldsymbol{r})\boldsymbol{v}_{\mathrm{f/s}}(\boldsymbol{r})$.

Chapter 5

Conclusions

In this work, we considered an active mixture of fast and slow swimmers in the presence of flat walls and asymmetric obstacles (with a curved and a flat side). We identified wetting and segregation in both systems, and rectification and vorticity for the asymmetric obstacles. Using simulations and theory, we showed how the degree of diversity of self-propulsion speeds, alters these phenomena, both quantitatively and qualitatively. We use δ to quantify the degree of speed diversity. For $\delta = 0$, all particles have identical self-propulsion speed and the system is called "monodisperse". In the opposite limit, when $\delta = 1$, the mixture is active-passive.

In the flat-wall case, we found that segregation is present throughout the dynamical evolution and that it consists of two stages. First, there is a fast dynamics, which occurs while particles are accumulating on the walls, and is characterized by a difference in the rate of absorption between the two particle types. In the active-passive case, a wind of active particles moving towards the wall pushes passive particles onto the layer. Second, a slow segregation dynamics, characterized by the relaxation of the layer. For $0.3 \leq \delta \leq 0.8$, it consists mostly of evaporation of a few fast particles and their substitution via absorption of slow particles. For $\delta < 0.3$ and $\delta > 0.8$, it consists of evaporation of both fast and slow particles.

Also, we determined via simulations the mean thickness of the layer by finding the biggest connected component of particles in contact and calculating the corresponding mean interface-wall distance as well as by using an orientation parameter

together with the fact that the particles point towards the wall at the interface of the wetting layer. We found excellent agreement between the two methods. In the steady state, we find that the mean thickness of the wetting layer decreases with δ. This is similar to previous results in the literature for analogous but distinct systems where active mixtures clusterize [18]. We developed a kinetic theory that captures that behavior. This approach allowed us to predict also the composition of the layer within the steady state and how it is affected by speed diversity. We applied the theory to obtain the transient and identified the need to incorporate "wind" or dragging effects in order to properly account for an overshoot in the mean thickness during its evolution.

In both systems, we found that the fast particles accumulate closer to the wall/obstacle and slow particles tend to accumulate farther from the wall/obstacle and, for sufficiently high δ, even on the layer of fast particles, provided that their low persistence do not allow them to penetrate further. The segregation parameter increases with δ but we find that total segregation is never achieved since in all cases there is an overlap of the fast and slow concentration profiles in the gas. The concentration profiles for $\delta = 0.9$ are significantly different from the passive-active case $\delta = 1$ since the persistence length for $\delta = 0.9$ is still comparable to the relevant sizes of the system such as the wetting layer and the obstacle size.

Regarding interactions with the asymmetric obstacle and the corresponding rectification, our results complement the explanation given in Ref. [33] for monodisperse systems: particles coming from the left side become rectified when sliding along the curved side of the obstacle, whereas those coming from the right side are oriented due to the formation of vortices which rotate favorably to the global current near the corners. Also since complete segregation is not achieved in the active-passive case, passive particles continue to rectify as they are pushed by the active ones. The mean current increases with δ since for fast particles the response to increasing their velocity is stronger than linear.

In the future, one could also investigate the above behaviors for distinct obstacle shapes or types of mixtures. For instance, the case of particle types with identical self-propulsion speeds but diverse in terms of rotational diffusivities would probably generate an amplification of wetting layers with diversity [18]. Another interesting research avenue is to include alignment forces, which, in principle, would make the rate of emission of particles decrease since it would be harder for particles to reorient towards the gas (although avalanche effects would be more pronounced and the behavior might depend non-trivially on that too). This thesis and these future investigations are expected to be useful to researchers studying the behavior of more realistic active matter systems such as bacterial fluids interacting with real surfaces.

Bibliography

[1] Sriram Ramaswamy. The mechanics and statistics of active matter. *Annu. Rev. Condens. Matter Phys.*, 1(1):323–345, 2010.

[2] Clemens Bechinger, Roberto Di Leonardo, Hartmut Löwen, Charles Reichhardt, Giorgio Volpe, and Giovanni Volpe. Active particles in complex and crowded environments. *Reviews of Modern Physics*, 88(4):045006, 2016.

[3] M. Ballerini, N. Cabibbo, R. Candelier, A. Cavagna, E. Cisbani, I. Giardina, V. Lecomte, A. Orlandi, G. Parisi, A. Procaccini, M. Viale, and V. Zdravkovic. Interaction ruling animal collective behavior depends on topological rather than metric distance: Evidence from a field study. *Proceedings of the National Academy of Sciences*, 105(4):1232–1237, 2008.

[4] Yael Katz, Kolbjørn Tunstrøm, Christos C. Ioannou, Cristián Huepe, and Iain D. Couzin. Inferring the structure and dynamics of interactions in schooling fish. *Proceedings of the National Academy of Sciences*, 108(46):18720–18725, 2011.

[5] Iztok Lebar Bajec and Frank H Heppner. Organized flight in birds. *Animal Behaviour*, 78(4):777–789, 2009.

[6] Fernanda Pérez-Verdugo, Jean-Francois Joanny, and Rodrigo Soto. Vertex model instabilities for tissues subject to cellular activity or applied stresses. *Physical Review E*, 102(5):052604, 2020.

[7] Andrey Sokolov, Igor S. Aranson, John O. Kessler, and Raymond E. Goldstein. Concentration dependence of the collective dynamics of swimming bacteria. *Physical Review Letters*, 98:158102, 04 2007.

[8] Ivo Buttinoni, Julian Bialké, Felix Kümmel, Hartmut Löwen, Clemens Bechinger, and Thomas Speck. Dynamical clustering and phase separation in suspensions of self-propelled colloidal particles. *Physical Review Letters*, 110:238301, 01 2013.

[9] Juliane Simmchen, Jaideep Katuri, William E Uspal, Mihail N Popescu, Mykola Tasinkevych, and Samuel Sánchez. Topographical pathways guide chemical microswimmers. *Nature Communications*, 7(1):1–9, 2016.

[10] Anrdás Búzás, Lóránd Kelemen, Anna Mathesz, László Oroszi, Gaszton Vizsnyiczai, Tamás Vicsek, and Pál Ormos. Light sailboats: Laser driven autonomous microrobots. *Applied Physics Letters*, 101(4):041111, 2012.

[11] Alan CH Tsang, Ebru Demir, Yang Ding, and On Shun Pak. Roads to smart artificial microswimmers. *Advanced Intelligent Systems*, 2(8):1900137, 2020.

[12] Yingjie Wu, Xiankun Lin, Zhiguang Wu, Helmuth Moehwald, and Qiang He. Self-propelled polymer multilayer janus capsules for effective drug delivery and light-triggered release. *ACS Applied Materials & Interfaces*, 6, 06 2014.

[13] Arijit Ghosh, Weinan Xu, Neha Gupta, and David H. Gracias. Active matter therapeutics. *Nano Today*, 31:100836, 2020.

[14] Michael E Cates and Julien Tailleur. Motility-induced phase separation. *Annu. Rev. Condens. Matter Phys.*, 6(1):219–244, 2015.

[15] Gabriel S. Redner, Michael F. Hagan, and Aparna Baskaran. Structure and dynamics of a phase-separating active colloidal fluid. *Physical Review Letters*, 110:055701, 01 2013.

[16] Néstor Sepúlveda and Rodrigo Soto. Wetting transitions displayed by persistent active particles. *Physical Review Letters*, 119(7):078001, 2017.

[17] René Wittmann and Joseph M Brader. Active brownian particles at interfaces: An effective equilibrium approach. *Europhysics Letters*, 114(6):68004, 2016.

[18] Pablo de Castro, Saulo Diles, Rodrigo Soto, and Peter Sollich. Active mixtures in a narrow channel: Motility diversity changes cluster sizes. *Soft Matter*, 17(8):2050–2061, 2021.

[19] Francesco Turci and Nigel B Wilding. Wetting transition of active brownian particles on a thin membrane. *arXiv preprint arXiv:2111.02492*, 2021.

[20] Rodrigo Soto and Ramin Golestanian. Run-and-tumble dynamics in a crowded environment: Persistent exclusion process for swimmers. *Physical Review E*, 89(1):012706, 2014.

[21] Pin Nie, Francisco Alarcon, Iván López-Montero, Belén Orgaz, Chantal Valeriani, and Massimo Pica Ciamarra. In-silico modeling of early-stage biofilm formation. *Soft Materials*, pages 1–13, 2021.

[22] Giordano Fausti, Elsen Tjhung, Michael Cates, and Cesare Nardini. Capillary interfacial tension in active phase separation. *arXiv preprint arXiv:2103.15563*, 2021.

[23] Iago Grobas, Marco Polin, and Munehiro Asally. Swarming bacteria undergo localized dynamic phase transition to form stress-induced biofilms. *bioRxiv*, 2020.

[24] Sameer Kumar, Jay Prakash Singh, Debaprasad Giri, and Shradha Mishra. Effect of polydispersity on the dynamics of active brownian particles. *Physical Review E*, 104(2):024601, 2021.

[25] Néstor Sepúlveda and Rodrigo Soto. Wetting transitions displayed by persistent active particles. *Physical Review Letters*, 119:078001, 08 2017.

[26] CJ Olson Reichhardt and Charles Reichhardt. Ratchet effects in active matter systems. *Annual Review of Condensed Matter Physics*, 8:51–75, 2017.

[27] Peter Reimann. Brownian motors: noisy transport far from equilibrium. *Physics Reports*, 361(2-4):57–265, 2002.

[28] Peter Galajda, Juan Keymer, Paul Chaikin, and Robert Austin. A wall of funnels concentrates swimming bacteria. *Journal of Bacteriology*, 189(23):8704–8707, 2007.

[29] Pulak K Ghosh, Vyacheslav R Misko, Fabio Marchesoni, and Franco Nori. Self-propelled janus particles in a ratchet: Numerical simulations. *Physical Review Letters*, 110(26):268301, 2013.

[30] Andrey Pototsky, Aljoscha M Hahn, and Holger Stark. Rectification of self-propelled particles by symmetric barriers. *Physical Review E*, 87(4):042124, 2013.

[31] Joakim Stenhammar, Raphael Wittkowski, Davide Marenduzzo, and Michael E Cates. Light-induced self-assembly of active rectification devices. *Science Advances*, 2(4):e1501850, 2016.

[32] Wei-jing Zhu, Teng-Chao Li, Wei-rong Zhong, and Bao-quan Ai. Rectification and separation of mixtures of active and passive particles driven by temperature difference. *The Journal of Chemical Physics*, 152(18):184903, 2020.

[33] Fabricio Q Potiguar, GA Farias, and WP Ferreira. Self-propelled particle transport in regular arrays of rigid asymmetric obstacles. *Physical Review E*, 90(1):012307, 2014.

[34] AD Borba, Jorge LC Domingos, ECB Moraes, FQ Potiguar, and WP Ferreira. Controlling the transport of active matter in disordered lattices of asymmetrical obstacles. *Physical Review E*, 101(2):022601, 2020.

[35] Iván Berdakin, Alejandro V Silhanek, Hernán N Moyano Cortéz, Verónica I Marconi, and Carlos A Condat. Quantifying the sorting efficiency of self-propelled run-and-tumble swimmers by geometrical ratchets. *Central European Journal of Physics*, 11(12):1653–1661, 2013.

[36] Jessé Pereira de Oliveira. Transporte em um sistema binário de partículas autopropelidas. 2015.

[37] Emiliano Perez Ipiña, Stefan Otte, Rodolphe Pontier-Bres, Dorota Czerucka, and Fernando Peruani. Bacteria display optimal transport near surfaces. *Nature Physics*, 15(6):610–615, 2019.

[38] Howard C Berg. *E. coli in Motion*. Springer Science & Business Media, 2008.

[39] Javier Sparacino, Gastón L Miño, Adolfo J Banchio, and VI Marconi. Solitary choanoflagellate dynamics and microconfined directed transport. *Journal of Physics D: Applied Physics*, 53(50):505403, 2020.

[40] Pablo de Castro and Peter Sollich. Phase separation dynamics of polydisperse colloids: a mean-field lattice-gas theory. *Phys. Chem. Chem. Phys.*, 19:22509–22527, 2017.

[41] Pablo de Castro and Peter Sollich. Critical phase behavior in multi-component fluid mixtures: Complete scaling analysis. *The Journal of Chemical Physics*, 149(20):204902, 2018.

[42] Pablo de Castro and Peter Sollich. Phase separation of mixtures after a second quench: composition heterogeneities. *Soft Matter*, 15(45):9287–9299, 2019.

[43] Pablo Souza de Castro Melo. *Phase separation of polydisperse fluids.* King's College London, 2019.

[44] Joakim Stenhammar, Raphael Wittkowski, Davide Marenduzzo, and Michael E Cates. Activity-induced phase separation and self-assembly in mixtures of active and passive particles. *Physical Review Letters*, 114(1):018301, 2015.

[45] Naveen Kumar Agrawal and Pallab Sinha Mahapatra. Alignment-mediated segregation in an active-passive mixture. *Physical Review E*, 104(4):044610, 2021.

[46] Thomas Kolb and Daphne Klotsa. Active binary mixtures of fast and slow hard spheres. *Soft Matter*, 16(8):1967–1978, 2020.

[47] Christian Hoell, Hartmut Löwen, and Andreas M Menzel. Multi-species dynamical density functional theory for microswimmers: Derivation, orientational ordering, trapping potentials, and shear cells. *The Journal of Chemical Physics*, 151(6):064902, 2019.

[48] Raphael Wittkowski, Joakim Stenhammar, and Michael E Cates. Nonequilibrium dynamics of mixtures of active and passive colloidal particles. *New Journal of Physics*, 19(10):105003, 2017.

[49] Sho C Takatori and John F Brady. A theory for the phase behavior of mixtures of active particles. *Soft Matter*, 11(40):7920–7931, 2015.

[50] AY Grosberg and J-F Joanny. Nonequilibrium statistical mechanics of mixtures of particles in contact with different thermostats. *Physical Review E*, 92(3):032118, 2015.

[51] AI Curatolo, N Zhou, Y Zhao, C Liu, A Daerr, J Tailleur, and J Huang. Cooperative pattern formation in multi-component bacterial systems through reciprocal motility regulation. *Nature Physics*, pages 1–6, 2020.

[52] Yan Wang, Zhuanglin Shen, Yiqi Xia, Guoqiang Feng, and Wende Tian. Phase separation and super diffusion of binary mixtures of active and passive particles. *Chinese Physics B*, 29(5):053103, 2020.

[53] Berend van der Meer, Vasileios Prymidis, Marjolein Dijkstra, and Laura Filion. Predicting the phase behavior of mixtures of active spherical particles. *The Journal of Chemical Physics*, 152(14):144901, 2020.

[54] Pritha Dolai, Aditi Simha, and Shradha Mishra. Phase separation in binary mixtures of active and passive particles. *Soft Matter*, 14(29):6137–6145, 2018.

[55] Andrea Villa-Torrealba, Cristóbal Chávez-Raby, Pablo de Castro, and Rodrigo Soto. Run-and-tumble bacteria slowly approaching the diffusive regime. *Physical Review E*, 101:062607, Jun 2020.

[56] Friederike Schmid and NB Wilding. Wetting of a symmetrical binary fluid mixture on a wall. *Physical Review E*, 63(3):031201, 2001.

[57] Willow R DiLuzio, Linda Turner, Michael Mayer, Piotr Garstecki, Douglas B Weibel, Howard C Berg, and George M Whitesides. Escherichia coli swim on the right-hand side. *Nature*, 435(7046):1271–1274, 2005.

[58] Allison P Berke, Linda Turner, Howard C Berg, and Eric Lauga. Hydrodynamic attraction of swimming microorganisms by surfaces. *Physical Review Letters*, 101(3):038102, 2008.

[59] Fernando Peruani, Jörn Starruß, Vladimir Jakovljevic, Lotte Søgaard-Andersen, Andreas Deutsch, and Markus Bär. Collective motion and nonequilibrium cluster formation in colonies of gliding bacteria. *Physical Review Letters*, 108(9):098102, 2012.

[60] Kenneth W. Desmond and Eric R. Weeks. Random close packing of disks and spheres in confined geometries. *Physical Review E*, 80:051305, Nov 2009.

[61] Pawel Romanczuk, Markus Bär, Werner Ebeling, Benjamin Lindner, and Lutz Schimansky-Geier. Active brownian particles. *The European Physical Journal Special Topics*, 202(1):1–162, 2012.

[62] Ryan C Maloney, Guo-Jun Liao, Sabine HL Klapp, and Carol K Hall. Clustering and phase separation in mixtures of dipolar and active particles. *Soft Matter*, 16(15):3779–3791, 2020.

[63] Nicholas Lauersdorf, Thomas Kolb, Moslem Moradi, Ehsan Nazockdast, and Daphne Klotsa. Dependence of phase behavior and surface tension on particle stiffness for active brownian particles. *Soft Matter*, 2021.

[64] Ricardo Brito and Rodrigo Soto. Competition of brazil nut effect, buoyancy, and inelasticity induced segregation in a granular mixture. *The European Physical Journal Special Topics*, 179(1):207–219, 2009.

[65] Pablo de Castro, Francisco M. Rocha, Saulo Diles, Rodrigo Soto, and Peter Sollich. Diversity of self-propulsion speeds reduces motility-induced clustering in confined active matter. *Soft Matter*, pages –, 2021.

[66] Ahmad K. Omar, Zhen-Gang Wang, and John F. Brady. Microscopic origins of the swim pressure and the anomalous surface tension of active matter. *Physical Review E*, 101:012604, Jan 2020.

[67] Adam Wysocki and Heiko Rieger. Capillary action in scalar active matter. *Physical Review Letters*, 124:048001, Jan 2020.

[68] Shreyas Gokhale, Junang Li, Alexandre Solon, Jeff Gore, and Nikta Fakhri. Dynamic clustering of passive colloids in dense suspensions of motile bacteria. *arXiv preprint arXiv:2110.02294*, 2021.